Eur. Phys. J. C (2023) 83:715
https://doi.org/10.1140/epjc/s10052-023-11887-z

THE EUROPEAN PHYSICAL JOURNAL C

Regular Article - Theoretical Physics

ν Electroweak baryogenesis: the scalar singlet strikes back

E. Fernández-Martínez[1], **J. López-Pavón**[2], **J. M. No**[1], **T. Ota**[1], **S. Rosauro-Alcaraz**[3,a]

[1] Departamento de Física Teórica and Instituto de Física Teórica, IFT-UAM/CSIC, Universidad Autónoma de Madrid, Cantoblanco, 28049 Madrid, Spain
[2] Instituto de Física Corpuscular, Universidad de Valencia and CSIC, Edificio Insitutos Investigación, Catedrático José Beltrán 2, 46980 Paterna, Spain
[3] Pôle Théorie, Laboratoire de Physique des 2 Infinis Irène Joliot Curie (UMR 9012) CNRS/IN2P3, 15 rue Georges Clemenceau, 91400 Orsay, France

Received: 17 April 2023 / Accepted: 30 July 2023 / Published online: 9 August 2023

Abstract We perform a comprehensive scan of the parameter space of a general singlet scalar extension of the Standard Model to identify the regions which can lead to a strong first-order phase transition, as required by the electroweak baryogenesis mechanism. We find that taking into account bubble nucleation is a fundamental constraint on the parameter space and present a conservative and fast estimate for it so as to enable efficient parameter space scanning. The allowed regions turn out to be already significantly probed by constraints on the scalar mixing from Higgs signal strength measurements. We also consider the addition of new neutrino singlet fields with Yukawa couplings to both scalars and forming heavy (pseudo)-Dirac pairs, as in the linear or inverse Seesaw mechanisms for neutrino mass generation. We find that their inclusion does not alter the allowed parameter space from early universe phenomenology in a significant way. Conversely, there are allowed regions of the parameter space where the presence of the neutrino singlets would remarkably modify the collider phenomenology, yielding interesting new signatures in Higgs and singlet scalar decays.

1 Introduction

The origin of the observed Baryon Asymmetry of the Universe (BAU) is one of the fundamental open problems of the Standard Model (SM) of particle physics and one of the few precious pieces of experimental evidence for physics beyond the SM together with the existence of neutrino masses and dark matter. The generation of the BAU in the early Universe requires satisfying the three Sakharov conditions [1]: baryon number violation, C and CP violation, and departure from thermal equilibrium. In principle the SM itself could address the origin of the BAU via the electroweak baryogenesis (EWBG) mechanism [2–7]. However, the SM three-family quark mixing encoded in the Cabibbo–Kobayashi–Maskawa (CKM) matrix does not provide enough CP violation to generate a sufficient asymmetry [8–10], and the early Universe transition from the electroweak (EW) symmetric phase to the EW broken phase in the SM is a smooth crossover [11,12], rather than the strongly first-order transition required by the out-of-equilibrium Sakharov condition.

Nevertheless, simple extensions of the SM could solve these issues and make EWBG viable. In particular, extending the scalar sector of the SM by just a real singlet field could allow for a first-order EW phase transition (see e.g. [13–17]). This new scalar singlet may not be alone, but rather be part of an extended dark sector to which it couples. A particularly motivated such scenario is the extension of the SM by (heavy) fermion singlets, i.e. right-handed neutrinos, able to account for the observed pattern of neutrino masses and mixings in Nature. Remarkably, it was shown in Refs. [18,19] that the new sources of CP violation that arise in this extension of the SM, from the simultaneous presence of Yukawa interactions of the heavy neutrinos with the singlet scalar and with the Higgs doublet and SM neutrinos, could lead to successful EWBG depending on the evolution of the scalar sector during the phase transition (a scenario referred to as ν-EWBG in [19]).

In this work we aim to clarify the conditions on the singlet scalar dynamics during the EW phase transition that possibly allows for EWBG in the above setup. Our scope is however more general, and we study the regions of parameter space of the real singlet scalar extension of the SM yielding a strong first-order phase transition (SFOPT), exploring the correlations among different model parameters, and emphasizing

[a] e-mail: rosauro@ijclab.in2p3.fr (corresponding author)

those that might arise between measurable quantities. The aim here is not a high-precision computation of the various thermodynamic quantities of the phase transition, which would be numerically challenging if combined with a thorough scan of the model parameter space. Rather, we focus on exploring the parameter space as efficiently as possible, covering broad areas of the multidimensional space via a number of approximations. Even if these approximations are not suitable to obtain highly-accurate results for the SFOPT quantities, they allow to pinpoint the regions of the parameter space with the desired features and test whether they are presently allowed, for subsequent analyses to concentrate in these regions. We pay particular attention to the SFOPT requirement of bubble nucleation for a successful completion of the EW phase transition, for which we provide conservative and fast estimate for assessing if nucleation would take place. While the nucleation dynamics has been studied previously [20] in the context of a $\mathbb{Z}_2$-symmetric singlet scalar extension of the SM, here we aim at a more general study without the additional constraint of additional symmetries. To the best of our knowledge, this is the first full scan exploring all the different correlations of the parameter space of the scalar singlet extension of the SM aiming to identify the regions where a SFOPT could take place. In addition, we investigate the impact of the heavy neutrinos on the SFOPT dynamics: while previous studies indicate that sizable values of the neutrino Yukawa interactions with the scalar singlet can strengthen the first-order phase transition [21], we find that large values of the neutrino Yukawas, unless compensated by other parameters, can also have the effect of destabilizing the EW broken minimum and are thus generally disfavoured. However, their inclusion does not alter significantly the allowed regions of the parameter space as compared to the singlet-only case.

Finally, we also discuss the phenomenological impact of the existence of such heavy neutrinos as compared to the minimal singlet scalar extension of the SM, finding that the phenomenology can be altered dramatically with respect to the latter model. Specifically, we find that the singlet-like scalar will dominantly decay into right-handed neutrinos (if allowed by phase space), instead of directly decaying into SM particles. These heavy neutrinos may then subsequently decay into SM particles either promptly or via displaced vertexes, depending on the size of their mixing θ with the active SM neutrinos. Since the production of the right-handed neutrinos from the scalar singlet decay is unrelated to the strongly constrained mixing θ, this heavy neutrino production process could well be the dominant one at colliders like the LHC. Besides, the mixing between the scalar singlet and the Higgs would also lead to exotic Higgs decays into right-handed neutrinos (if these are light enough), which can be probed via Higgs signal strength measurements and also in direct searches for such exotic Higgs decays (see e.g. [22]) at the LHC.

This paper is organized as follows. In Sect. 2 we introduce the real singlet scalar extension of the SM with the addition of heavy neutrinos, and discuss the details of the scalar potential in the early Universe relevant for our SFOPT analysis. Then, in Sect. 3 we analyze the experimental constraints on the model, as well as the possible new combined probes of the existence of the singlet and the heavy neutrinos. In Sect. 4 we give details of our model parameter scan, and we discuss its results in Sect. 5. We finally conclude in Sect. 6.

2 The scalar singlet extension of the SM with heavy neutrinos

The simplest extension of the SM scalar sector is the inclusion of a real scalar singlet s that may mix with the Higgs boson. This small addition to the SM may however significantly alter the scalar sector phenomenology. In particular, it can allow for a SFOPT even at tree-level [13,15], re-opening the possibility of explaining the origin of the observed matter–antimatter asymmetry of the Universe in the context of EWBG if new sources of CP violation beyond the SM are also present.

More interestingly, the scalar singlet field s could be a window to a dark sector capable of addressing some of the other open problems of the SM. Indeed, given its singlet nature, renormalizable (and therefore less suppressed) couplings are expected between the scalar and both the SM and the extended dark sector. Such scenarios could for example account for the observed dark matter of the Universe [23] (see also [24–31]) or the simultaneous origin of neutrino masses and the BAU [18,19]. Motivated by the latter, but easily generalizable, in this work we will consider a dark sector that comprises the real scalar field s and n new Dirac neutrinos, $N' = (N'_L, N'_R)$, singlets under the SM gauge group and with lepton number $+1$. In order to have an accessible extended neutrino sector with masses around the EW scale that may play a non-trivial role in the SFOPT and the baryogenesis process, we consider low-scale realizations of the Seesaw mechanism [32–35] with an approximate lepton number conservation so as to protect and ensure the lightness of neutrino masses [36–38]. Indeed in the so-called inverse [39,40] or linear [41,42] Seesaw mechanisms the new heavy neutrinos arrange in Dirac pairs while the SM neutrinos remain massless if the lepton number symmetry is exact. Upon softly breaking this symmetry, the SM neutrinos will acquire small masses and the mass degeneracy of the two members of each Dirac pair will be slightly broken [43]. Neglecting the small lepton-number-violating terms (which are suppressed by the tiny SM neutrino masses), the most general lepton-

number-conserving interaction Lagrangian among the dark sector fields s, N' and the SM fields is:

$$\mathcal{L} \supset \left(-\overline{L_L}\tilde{\Phi} Y_\nu N'_R - \overline{N'_L}\, s Y_N N'_R + h.c.\right) + V\left(\Phi^\dagger\Phi, s\right), \tag{2.1}$$

where Φ is the $SU(2)_L$ doublet Higgs field, $\tilde{\Phi} = i\sigma_2\Phi^*$, L_L is the $SU(2)_L$ lepton doublet and Y_ν and Y_N are general $3\times n$ and $n\times n$ Yukawa matrices, respectively. Without loss of generality we will work in the basis where Y_N is diagonal.

The most general Lagrangian scalar potential for the Higgs doublet Φ and the singlet scalar s is given by (see e.g. [15])

$$\begin{aligned} V\left(\Phi^\dagger\Phi, s\right) = &-\tilde{\mu}_h^2\Phi^\dagger\Phi + \lambda_h(\Phi^\dagger\Phi)^2 \\ &+\frac{1}{2}\tilde{\mu}_s^2 s^2 + \frac{1}{4}\lambda_s s^4 \\ &+\frac{1}{2}\mu_m s\Phi^\dagger\Phi + \frac{1}{2}\lambda_m s^2\Phi^\dagger\Phi \\ &+\tilde{\mu}_1^3 s + \frac{1}{3}\mu_3 s^3. \end{aligned} \tag{2.2}$$

By writing $\Phi = (h^+, (h + i\chi)/\sqrt{2})$, the scalar potential for the neutral fields h and s, relevant for EW symmetry breaking, is found to be

$$\begin{aligned} V(h,s) = &-\frac{1}{2}\tilde{\mu}_h^2 h^2 + \frac{1}{4}\lambda_h h^4 + \frac{1}{2}\tilde{\mu}_s^2 s^2 + \frac{1}{4}\lambda_s s^4 \\ &+\frac{1}{4}\mu_m s h^2 + \frac{1}{4}\lambda_m s^2 h^2 + \tilde{\mu}_1^3 s + \frac{1}{3}\mu_3 s^3\,. \end{aligned} \tag{2.3}$$

In the rest of this work, we will denote the (zero-temperature) vacuum expectation values (vevs) of the Higgs and singlet fields stemming from the potential (2.3) by v_{EW} and ω_{EW}, respectively. We note that all parameters from $V(h,s)$ are real, which means that the only sources of CP violation beyond the SM would arise from the Yukawa couplings in Eq. (2.1), in the absence of further new physics contributions.

In general, to study the early Universe dynamics of the scalar sector and the possibility to have a SFOPT, zero-temperature loop corrections (at 1-loop, this corresponds to the so-called Coleman–Weinberg contribution [44]) as well as finite-temperature contributions to the scalar potential [45,46], should be taken into account. These corrections, however, introduce gauge dependence [47] and renormalization scale dependence in the effective potential of the theory, leading to important theoretical uncertainties [48,49].[1] Nevertheless, the scalar potential of the singlet scalar extension of the SM may already lead to the generation of a tree-level barrier between the EW symmetric and broken minima [15] and, in such a case, an analysis based on the tree-level potential (2.3) supplemented by the leading ($\sim T^2$) thermal corrections in a high-temperature approximation, which do not depend on the choice of the gauge, captures the most relevant features needed for the study of the SFOPT. At the same time, working at this level of approximation allows to study the relevant features of the phase transition analytically, as advocated in Ref. [15]. This is very advantageous in order to efficiently scan the parameter space of the model. We have verified the generic validity of this approximation concerning the results of our global parameter scan, as we discuss in more detail in Sect. 4. The finite-temperature effective potential V_T can in this case be written as:

$$\begin{aligned} V_T(h,s,T) = &-\frac{1}{2}\mu_h^2 h^2 + \frac{1}{4}\lambda_h h^4 + \frac{1}{2}\mu_s^2 s^2 + \frac{1}{4}\lambda_s s^4 \\ &+\frac{1}{4}\mu_m s h^2 + \frac{1}{4}\lambda_m s^2 h^2 + \mu_1^3 s + \frac{1}{3}\mu_3 s^3 \\ &+\left[\frac{1}{2}c_h h^2 + \frac{1}{2}c_s s^2 + m_3 s\right](T^2 - T_c^2). \end{aligned} \tag{2.4}$$

The explicit appearance as a free parameter in Eq. (2.4) of the critical temperature T_c, at which the EW symmetric and broken minima are degenerate in energy, proves very convenient in a scan of the model parameter space requiring the presence of a SFOPT. Indeed, when imposing that at $T = T_c$ the two minima are degenerate, an analytical condition among the other potential parameters in Eq. (2.4) is obtained, effectively trading its freedom for T_c and allowing to explore only potentials for which the two-degenerate-minima condition is fulfilled (see Appendix A for details). The parameters in Eq. (2.4), defined at $T = T_c$, are related to those of Eq. (2.3), defined at $T = 0$, by $\tilde{\mu}_h^2 \equiv \mu_h^2 + c_h T_c^2$, $\tilde{\mu}_s^2 \equiv \mu_s^2 - c_s T_c^2$, and $\tilde{\mu}_1^3 \equiv \mu_1^3 - m_3 T_c^2$. The constants c_h, c_s and m_3 are given by

$$\begin{aligned} c_h &= \frac{1}{48}\left[9g^2 + 3g'^2 + 2(6Y_t^2 + 12\lambda_h + \lambda_m + 2\mathcal{Y}_\nu^2)\right], \\ c_s &= \frac{1}{12}\left[2\lambda_m + 3\lambda_s + 2\mathcal{Y}_N^2\right], \\ m_3 &= \frac{1}{12}\left[\mu_3 + \mu_m\right], \end{aligned} \tag{2.5}$$

where g and g' are respectively the $SU(2)_L$ and $U(1)_Y$ gauge couplings, Y_t is the top Yukawa coupling, and $\mathcal{Y}_\nu^2$, $\mathcal{Y}_N^2$ are defined as $\mathcal{Y}_\nu^2 \equiv \mathrm{tr}\left(Y_\nu^\dagger Y_\nu\right)$, $\mathcal{Y}_N^2 \equiv \mathrm{tr}\left(Y_N^\dagger Y_N\right)$.

For the study of the temperature evolution of the scalar potential minima and the SFOPT, it is also convenient to rewrite the potential V_T from Eq. (2.4) in terms of the temperature-dependent vevs $v_T \equiv \langle h\rangle(T)$ and $\omega_T \equiv \langle s\rangle(T)$ in the broken minimum as [15]

[1] A possibility to alleviate these problems consists of performing dimensional reduction, working with a 3-dimensional effective theory [50–54]. This procedure consists in practice on successively integrating-out all the heavy energy scales of the system (see e.g. [48] for a recent discussion on the topic).

$$
\begin{aligned}
V_T(h,s,T) = & \frac{m_h^2}{8v_T^2}\left(h^2-v_T^2\right)^2 \\
& + \frac{m_{sh}^2}{2v_T}\left(h^2-v_T^2\right)(s-\omega_T) \\
& + \frac{1}{4}\left[2m_s^2+\lambda_m\left(h^2-v_T^2\right)\right](s-\omega_T)^2 \\
& + \frac{v_T}{2m_h^2}\left(\lambda_m m_{sh}^2+4m_*\right)(s-\omega_T)^3 \\
& + \frac{v_T^2}{8m_h^2}\left(4\lambda^2+\lambda_m^2\right)(s-\omega_T)^4 , \qquad (2.6)
\end{aligned}
$$

where all dimensionful parameters have an implicit dependence on the temperature T. The mass parameters m_h^2, m_s^2, and m_{sh}^2 are defined as

$$
\begin{aligned}
& m_h^2 \equiv \left.\frac{\partial^2 V}{\partial h \partial h}\right|_{(v_T,\omega_T)}, \quad m_s^2 \equiv \left.\frac{\partial^2 V}{\partial s \partial s}\right|_{(v_T,\omega_T)}, \\
& m_{sh}^2 \equiv \left.\frac{\partial^2 V}{\partial h \partial s}\right|_{(v_T,\omega_T)}, \qquad (2.7)
\end{aligned}
$$

evaluated at the EW broken minimum at T. The effective coupling λ^2 and mass m_* in Eq. (2.6) are defined as

$$
\begin{aligned}
\lambda^2 \equiv & \lambda_h\lambda_s - \frac{1}{4}\lambda_m^2, \quad m_* \equiv \lambda^2\omega_T \\
& + \frac{1}{3}\lambda_h\mu_3 - \frac{1}{8}\lambda_m\mu_m . \qquad (2.8)
\end{aligned}
$$

Furthermore, in the parameter scans in Sect. 4 we will eventually trade m_{sh}^2 for the quantity ω_p, defined as

$$
\omega_p \equiv \omega_T - \frac{m_{sh}^2}{\lambda_m v_T} = \frac{-\mu_m}{2\lambda_m}, \qquad (2.9)
$$

which has the advantage of being temperature-independent. The parametrization (2.6) explicitly shows that a shift in the field $s \to s+\sigma$ keeps the finite-temperature scalar potential V_T invariant with a redefinition of $\omega_T \to \omega_T+\sigma$. The relations between the new parameters in Eq. (2.6) and the coefficients in Eq. (2.3) are found in Ref. [15].

The starting point of our analysis of SFOPT scenarios is the finite-temperature potential V_T from Eq. (2.4) at $T=T_c$, with two degenerate minima located in general at $(0,\omega_0)$ and $(v,\omega) \equiv (v_{T_c},\omega_{T_c})$ in the two-dimensional field space. We will require that both the Higgs and the singlet field acquire a vev in the EW broken phase, in order to generate masses for the heavy neutrinos after the phase transition. Furthermore, in Ref. [19] it was shown that successful baryogenesis in the present scenario favours the heavy neutrinos to be approximately massless at the onset of the SFOPT. We will thus make use of the shift symmetry of the potential via $\omega_T \to \omega_T+\sigma$ discussed above to set $\omega_0=0$ at the critical temperature T_c (this corresponds to setting $\mu_1=0$ in Eq. (2.4)), and mainly focus on phase transitions from $(\langle h\rangle,\langle s\rangle) = (0,0) \to (v,\omega)$. For studies on other phase transition scenarios in the singlet scalar extension of the SM, we refer the reader to Refs. [17,20,49,55–63]. Following [15], we can use Eq. (2.6) to conveniently parametrize the finite-temperature potential at the critical temperature as

$$
\begin{aligned}
V_T(h,s,T_c) = & \frac{v^2 m_h^2}{8}\left\{\left(\frac{h^2}{v^2}-1\right)^2 + \left(\frac{s}{\omega}-1\right)^3\left(1+\frac{3s}{\omega}\right)\right. \\
& + 2\frac{\lambda_m\omega^2}{m_h^2}\left(\frac{s}{\omega}-1\right)^2\left(\frac{h^2}{v^2}-\frac{s^2}{\omega^2}\right) \\
& + \frac{4m_s^2}{m_h^2}\frac{s^2}{v^2}\left(\frac{s}{\omega}-1\right)^2 + \frac{4m_{sh}^2\omega}{m_h^2 v}\left(\frac{s}{\omega}-1\right) \\
& \left.\times\left[\frac{h^2}{v^2}+\frac{s^2}{\omega^2}\left(\frac{2s}{\omega}-3\right)\right]\right\}. \qquad (2.10)
\end{aligned}
$$

The set of parameters of Eq. (2.4) at $T=T_c$ can be recovered from the new parametrization given in Eq. (2.10) (together with $\mu_1=0$) via the following relations[2]:

$$
\mu_h^2 = \frac{1}{2}\left(m_h^2 - \lambda_m\omega^2 + 2\frac{\omega m_{sh}^2}{v}\right), \qquad (2.11)
$$

$$
\lambda_h = \frac{1}{2}\frac{m_h^2}{v^2}, \qquad (2.12)
$$

$$
\mu_s^2 = \frac{1}{2}\frac{v^2}{\omega^2}\left(3m_h^2 - \lambda_m\omega^2 + 2\frac{\omega^2 m_s^2}{v^2} + 6\frac{\omega m_{sh}^2}{v}\right), \qquad (2.13)
$$

$$
\lambda_s = \frac{1}{2}\frac{v^2}{\omega^4}\left(3m_h^2 - 2\lambda_m\omega^2 + 4\frac{\omega^2 m_s^2}{v^2} + 8\frac{\omega m_{sh}^2}{v}\right), \qquad (2.14)
$$

$$
\mu_m = -2\left(\omega\lambda_m - \frac{m_{sh}^2}{v}\right), \qquad (2.15)
$$

$$
\mu_3 = -\frac{3}{2}\frac{v^2}{\omega^3}\left(2m_h^2 - \lambda_m\omega^2 + 2\frac{\omega^2 m_s^2}{v^2} + 5\frac{\omega m_{sh}^2}{v}\right). \qquad (2.16)
$$

Then, the set of parameters $\{\omega, \omega_p, v, m_h^2, m_s^2, \lambda_m\}$ evaluated at $T=T_c$ is enough to fully characterize the scalar potential with two degenerate minima at $(0,0)$ and (v,ω).[3] Together with T_c, this set of parameters allows us to specify the finite-temperature potential as a function of T in the singlet scalar extension of the SM, in the high-T approximation. When considering the addition of extra heavy Dirac neutrinos, we also need to add $\mathcal{Y}_\nu$ and $\mathcal{Y}_N$ as free parameters in our analysis, since they appear in the thermal corrections of the potential V_T, see Eq. (2.5).

[2] These are only valid at $T=T_c$. We refer the reader to Ref. [15] for the general relation between both sets of parameters.

[3] We re-stress that we have already made use of the shift symmetry in the singlet field direction and taken $\omega_0=0$ without loss of generality, thus having 7 free parameters to describe the potential.

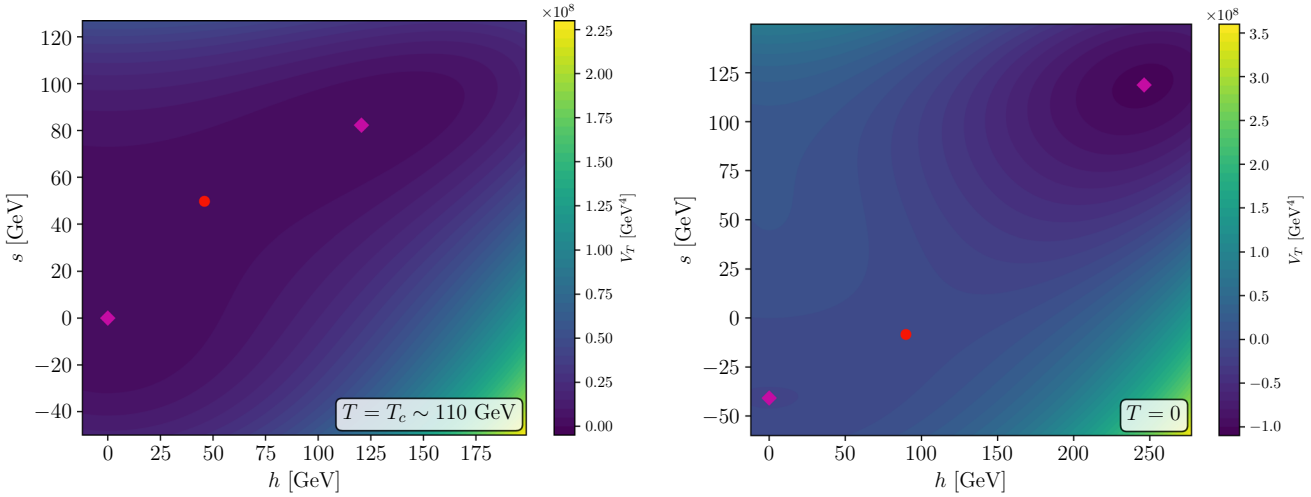

Fig. 1 Shape of the scalar potential for the example point in parameter space specified in Table 1 at the critical temperature T_c (left panel) and at $T = 0$ (right panel). The color bar denotes the value of the scalar potential, V_T. The purple diamonds denote the location of the minima, which are degenerate at T_c. The red dot denotes the location of the saddle point, which is close to the field trajectory for bubble nucleation (the bounce solution) at the nucleation temperature T_N (see Sect. 4 for details)

Table 1 Parameter set at $T = 0$ corresponding to the scalar potential shown in Fig. 1. This parameter set gives rise to a SFOPT with successful nucleation and satisfying all the bounds from Higgs phenomenology, including those on the scalar mixing (see Sect. 3 for details)

$\tilde{\mu}_h^2$ [GeV^2]	λ_h	$\tilde{\mu}_s^2$ [GeV^2]	λ_s	μ_m [GeV]	λ_m
1859.56	0.143276	−2076.39	1.9975	−164.272	0.415282
$\tilde{\mu}_1^3$ [GeV^3]	μ_3 [GeV]	$\mathcal{Y}_N$	ω_{EW} [GeV]	M_S [GeV]	$\sin\xi$
341158	−173.445	0.293868	118.772	236.786	0.207

Figure 1 illustrates an example of the type of scalar potentials that would lead to a SFOPT with the characteristics described above, with the specific values of the corresponding potential parameter set at $T = 0$ given in Table 1. In the left panel of Fig. 1, the potential $V_T(h, s, T)$ is shown at $T = T_c$ with the two degenerate minima, represented by the purple diamonds. The red dot indicates the location of the saddle point yielding a potential barrier between both minima. In the right panel we show the potential at $T = 0$ where the EW breaking minimum (v_{EW}, ω_{EW}) is now the true vacuum and also the real singlet has an $\mathcal{O}(100$ GeV) vev that generates EW-scale masses for the heavy neutrinos.

In general, the potential V_T from Eq. (2.10) characterized by a random set of parameters $\{\omega, \omega_p, v, m_h^2, m_s^2, \lambda_m\}$ at T_c satisfying the conditions in Appendix A from Ref. [15], despite satisfying the desired property of featuring two degenerate minima at $(0, 0)$ and (v, ω), will not reproduce the correct value for the EW symmetry breaking vev at $T = 0$, $v_{EW} = 246.22$ GeV, obtained from the measurement of the Fermi constant via the muon decay width [64]. In addition, upon diagonalization of the scalar mass matrix at $T = 0$,

$$\mathcal{M}_s^0 = \begin{pmatrix} m_h^2 & m_{sh}^2 \\ m_{sh}^2 & m_s^2 \end{pmatrix}\Bigg|_{T=0}, \tag{2.17}$$

with m_h^2, m_s^2 and m_{sh}^2 defined in Eq. (2.7) and evaluated in the $T = 0$ EW broken minimum (v_{EW}, ω_{EW}), the eigenvalue M_H for the mostly-doublet mass eigenstate will generally not reproduce the measured value for the Higgs boson mass $M_H = 125.10$ GeV. Satisfying these two physical requirements at $T = 0$ is rather non-trivial in our setup, and considerably reduces the allowed parameter space: given the high accuracy of the v_{EW} and M_H measurements, two combinations of the free parameters in the scalar potential are effectively determined. In Sect. 4 we will discuss how these requirements are implemented in our numerical scan of the parameter space of the model.

Finally, we also need to consider the existing constraints on the mixing ξ between the Higgs doublet and the scalar singlet, arising from the diagonalisation of the $T = 0$ scalar mass matrix, $\mathcal{M}_s^0$. We have

$$\begin{aligned} h &= v_{EW} + \cos\xi\, H + \sin\xi\, S, \\ s &= \omega_{EW} - \sin\xi\, H + \cos\xi\, S, \end{aligned} \tag{2.18}$$

where S (H) is the mass eigenstate corresponding to the mostly-singlet (doublet) scalar combination with a mass M_S ($M_H = 125.10$ GeV). In the next section we will discuss the present experimental constraints on the ($T = 0$) model parameters, affecting in particular the possible allowed values of the mixing ξ, which will also be applied to our parameter scan in Sect. 4.

3 Experimental constraints and phenomenological probes

In this section we discuss the relevant experimental limits on the singlet scalar extension of the SM, making emphasis on how the possible presence of the extra heavy singlet neutrinos can affect them. These experimental constraints will translate into bounds on the parameters of the potential from Eq. (2.4) at $T = 0$. We also discuss the main phenomenological probes of the model, particularly in connection with both the structure of the scalar potential and the presence of the heavy neutrinos in comparison with the minimal singlet scalar extension of the SM.

3.1 SM-heavy neutrino mixing

The new Dirac neutrinos with components N'_R and N'_L introduced in Eq. (2.1) mix with the SM neutrinos after spontaneous symmetry breaking (SSB) and may participate in the generation of light neutrino masses. The mixing matrix between the SM active and the heavy sterile neutrinos is given by

$$\theta \equiv \frac{v_{EW}}{\sqrt{2}\,\omega_{EW}} Y_\nu Y_N^{-1}, \tag{3.1}$$

with the Yukawa matrices Y_N and Y_ν for singlet and SM neutrinos (see Eq. (2.1) for details), respectively. Thus, neglecting all small L-violating parameters that would eventually lead to the generation of the masses of the mostly SM-like light neutrinos, the heavy neutrinos have Dirac masses $M_{N_i} \simeq \omega_{EW} Y_{Ni}$ and the two chiralities of the mass eigenstates N_i are given by

$$N_R = N'_R, \quad N_L \simeq N'_L - \theta^\dagger \nu_L. \tag{3.2}$$

For sterile neutrinos with masses $M_{N_i} > M_W$, the active-sterile neutrino mixing is bounded from above by a combination of EW precision tests[4] and flavour observables [67,68]

$$\mathrm{tr}\left(\theta\theta^\dagger\right) < 0.0048 \quad (2\sigma). \tag{3.3}$$

For lighter sterile neutrinos ($M_{N_i} < M_W$), direct searches at colliders and beam dump experiments as well as searches for peaks and distortions in the decay products of mesons, leptons and beta decays set much more stringent constraints on the active-sterile neutrino mixing, and we refer the reader to Refs. [69,70] for a comprehensive list of these limits.

The bound (3.3) will be used as a χ^2 contribution added to the weight function that we construct to guide our scan of the parameter space (see Appendix A). To constrain $\mathcal{Y}_\nu^2 = \mathrm{tr}\left(Y_\nu^\dagger Y_\nu\right)$ in our parameter scan, we use that

$$\mathrm{tr}\left(\theta\theta^\dagger\right) \leq \frac{v_{EW}^2}{2\,\omega_{EW}^2} \mathcal{Y}_\nu^2\, \mathrm{tr}\left(Y_N^{-2}\right), \tag{3.4}$$

since $\mathrm{tr}\,(AB) \leq \mathrm{tr}\,(A)\,\mathrm{tr}\,(B)$. Thus, when imposing the present bound on $\mathrm{tr}\left(\theta\theta^\dagger\right)$ to the right-hand side of Eq (3.4), a conservative bound is implemented since $\mathrm{tr}\left(\theta\theta^\dagger\right)$ will always be smaller than this quantity. In practice, because we only have access to $\mathcal{Y}_N$ and not the individual values of the Yukawas, when constraining $\mathcal{Y}_\nu$ we assume a degenerate spectrum such that $\mathrm{tr}\left(Y_N^{-2}\right) = n^2 \mathcal{Y}_N^{-2}$. Any other choice would translate into smaller values for $\mathcal{Y}_\nu$.

3.2 LHC Higgs signal strengths

The latest measurements of the 125 GeV Higgs boson signal strength by the ATLAS [71] and CMS [72] collaborations provide an important constraint on deviations of Higgs couplings from their SM values. In the singlet scalar extension of the SM, all SM couplings to the Higgs-like mass eigenstate H become rescaled relative to the SM values by $\cos\xi$, which, in the absence of exotic Higgs decays (see discussion below), yields an overall suppression of Higgs signal strength given by

$$\mu \equiv \frac{\sigma \cdot BR}{(\sigma \cdot BR)_{SM}} = \cos^2\xi. \tag{3.5}$$

This allows to constrain the singlet-doublet scalar mixing via Higgs measurements (see [73–76]). We use the latest measurements of the Higgs signal strength from ATLAS, $\mu = 1.05 \pm 0.06$ [77] and CMS, $\mu = 1.002 \pm 0.057$ [78], and combine them to derive a bound on $\cos\xi$ following the Feldman–Cousins [79] prescription.[5] We find $\mu \geq 0.94$ at the 95% C.L. which translates into $|\sin\xi| < 0.245$, as shown in Fig. 2. This is in fairly good agreement with other recent analyses (see e.g. [76]) where Feldman–Cousins is however not applied in general.

In the presence of an exotic Higgs branching fraction into beyond-the-SM (BSM) states $\mathrm{BR}_{H\to\mathrm{BSM}}$, the Higgs signal strength modifier μ in Eq. (3.5) becomes

[4] Notice that the recent anomalous measurement of M_W by the CDF II collaboration [65] could be potentially explained through a non-zero neutrino mixing [66]. However, this result is in tension with the other observables and we conservatively do not take it into account here.

[5] We adopt the Feldman–Cousins method to incorporate in a consistent way the fact that the best fit value from [77,78], corresponding to $\mu > 1$, is not achievable in the scalar singlet extension of the SM.

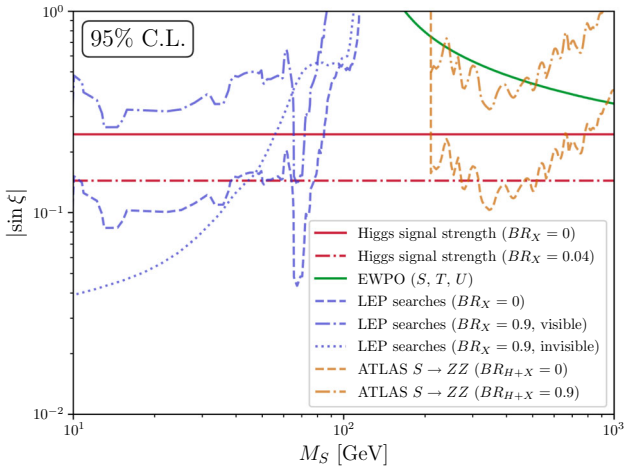

Fig. 2 Existing 95% C.L. constraints on the singlet-doublet scalar mixing $\sin\xi$ as a function of M_S from EWPO (solid green), from LHC Higgs signal strength measurements (red) with $\text{BR}_{H\to\text{BSM}} \equiv \text{BR}_X = 0$ (solid) and $\text{BR}_X = 0.04$ (dash-dotted), from direct searches for $pp \to S \to ZZ$ by ATLAS [83] (ocher), with $\text{BR}_{S\to HH} + \text{BR}_{S\to\text{BSM}} \equiv \text{BR}_{H+X} = 0$ (dashed) and $\text{BR}_{H+X} = 0.9$ (dash-dotted), and from LEP searches for light scalars (blue) respectively assuming $\text{BR}_{S\to\text{BSM}} \equiv \text{BR}_X = 0$ (dashed), $\text{BR}_X = 0.9$ with visible BSM decays (dash-dotted) and $\text{BR}_X = 0.9$ with invisible BSM decays (dotted)

$$\mu = \left(1 - \text{BR}_{H\to\text{BSM}}\right)\cos^2\xi \tag{3.6}$$

since $\cos\xi$ and $\text{BR}_{H\to\text{BSM}}$ now yield a combined dilution of the global Higgs signal strength with respect to the SM. Thus, the presence of exotic Higgs decays yield a tighter bound on $\cos^2\xi$ from Higgs signal strengths, as shown in Fig. 2 for the specific value $\text{BR}_{H\to\text{BSM}} \equiv \text{BR}_X = 0.04$[6]. In particular, the interactions in Eq. (2.1) between the Higgs boson H and the extra heavy neutrino states N_i could lead to $H \to N_i\bar{N}_i$ if $M_{N_i} < M_H/2$, with the heavy neutrino masses $M_{N_i} \simeq Y_{N_i}\,\omega_{EW}$. This occurs via Y_N in Eq. (2.1), through the singlet-doublet scalar mixing, or via Y_ν, through the active-sterile neutrino mixing. In addition, the interaction Y_ν may also mediate $H \to \nu\bar{N}_i$, $\bar{\nu}N_i$ decays [80,81]. Since the singlet-doublet scalar mixing is much more weakly constrained than the active-sterile neutrino mixing, the leading interaction (assuming $\theta^2 \ll \sin^2\xi$) after EW symmetry breaking between the scalar states and the N_i ($i = 1,\ldots,n$), which is induced by the Lagrangian from Eq. (2.1), would be

$$\mathcal{L} \supset \frac{1}{\omega_{EW}}(\cos\xi\, S - \sin\xi\, H)\sum_i \bar{N}_i M_{N_i} N_i. \tag{3.7}$$

The $H \to N_i\bar{N}_i$ decay channel is then driven by the scalar mixing, $\Gamma_{H\to N_i\bar{N}_i} \propto \sin^2\xi$, while in minimal seesaw scenarios the heavy neutrinos are produced via mixing with the SM neutrinos, leading to $\Gamma_{H\to N_i\bar{N}_i} \propto \theta^4$ and $\Gamma_{H\to\nu N_i} \propto \theta^2$. In our scenario these generally correspond to subleading effects (the corrections for both H and S interactions in Eq. (3.7) are $\mathcal{O}(\theta^2)$), and we concentrate in the following on the leading interaction from Eq. (3.7).

The decay $H \to N_i\bar{N}_i$ can have a significant impact on the LHC bounds on the Higgs signal strength. From the latest μ measurements performed by ATLAS [77] and CMS [78] and discussed above, we set the bound[7]

$$\left(1 - \sum_i \text{BR}_{H\to N_i\bar{N}_i}\right)\cos^2\xi \geq 0.94. \tag{3.8}$$

The total rate of the Higgs-like boson with a mass of 125 GeV decaying into N_i states is given by

$$\Gamma_{H\to N\bar{N}} \equiv \sum_{i=1}^{k}\Gamma_{H\to N_i\bar{N}_i} \simeq \frac{\sin^2\xi}{8\pi}M_H \times \sum_{i=1}^{k} Y_{N_i}^2\left(1 - \frac{4\,\omega_{EW}^2}{M_H^2}Y_{N_i}^2\right)^{3/2}, \tag{3.9}$$

where $k \leq n$ is the number of kinematically accessible heavy neutrinos. The maximum possible value of $\Gamma_{H\to N\bar{N}}$ (occurring for $k = n$) is given by

$$\Gamma_{\max} = n\,\frac{\sin^2\xi}{80\,\pi}\left(\frac{3}{5}\right)^{3/2}\frac{M_H^3}{\omega_{EW}^2} \simeq 10^{-2}\,\text{GeV} \times \left(\frac{n}{3}\right)\left(\frac{\sin^2\xi}{0.05}\right)\left(\frac{200\,\text{GeV}}{\omega_{EW}}\right)^2, \tag{3.10}$$

which is achieved for $Y_{N_i}^2 = M_H^2/(10\,\omega_{EW}^2)$ with $i = 1, 2, \ldots n$, and may well be comparable to the SM Higgs boson total width $\Gamma_{\text{SM}} = 0.00412$ GeV [82] if the mixing $\sin\xi$ is not too suppressed. For a given value of $\mathcal{Y}_N^2 = \sum_{i=1}^{n} Y_{N_i}^2$, which is the relevant combination of neutrino Yukawa couplings affecting the thermal history of the scalar sector, the following two "Cases" are possible:

1. $\boldsymbol{\mathcal{Y}_N^2\,\omega_{EW}^2 < (M_H/2)^2}$: Then all neutrinos are kinematically accessible and $k = n$ in Eq. (3.9) so that the 125 GeV Higgs boson decays into all n heavy neutrinos. For a fixed $\mathcal{Y}_N^2$ the maximum value of $\Gamma_{H\to N\bar{N}}$ is achieved when all Yukawa couplings are equal ($Y_{N_i}^2 = \mathcal{Y}_N^2/n$ with $i = 1, 2, \ldots n$), while the minimum value is obtained when the rate is dominated by a single heavy neutrino contribution ($Y_{N_1}^2 \approx \mathcal{Y}_N^2 \gg Y_{N_i}^2$ with $i = 2, \ldots n$).
2. $\boldsymbol{\mathcal{Y}_N^2\,\omega_{EW}^2 > (M_H/2)^2}$: The decay of the 125 GeV Higgs boson into at least one heavy neutrino may be kinemat-

[6] It is clear from (3.6) that an exotic branching fraction $\text{BR}_{H\to\text{BSM}} \geq 0.06$ is by itself ruled out at 95% C.L.

[7] We neglect $\text{BR}_{H\to\nu N_i}$ as discussed above. In addition, we neglect a possible branching fraction $\text{BR}_{H\to SS}$, potentially present only for very light singlets.

ically forbidden.[8] Therefore, for a given value of $\mathcal{Y}_N^2$, the decay rate can be arbitrarily suppressed depending on the value of the individual Yukawas Y_{N_i} (e.g. in the limit $Y_{N_1}^2 \to \mathcal{Y}_N^2$, $Y_{N_i}^2 \to 0$ for $i = 2, \ldots n$) and no lower bound on $\Gamma_{H\to N\bar{N}}$ exists. Still, sizable Higgs boson branching ratios into sterile neutrinos are also possible (even reaching $\Gamma_{H\to N\bar{N}} = \Gamma_{\max}$) in this case for a fixed value of $\mathcal{Y}_N^2$.

The inclusion of the exotic $H \to N\bar{N}$ decay channel on the Higgs signal strength bound (recall Eq. (3.8)) allows to exclude a significant fraction of the parameter space in which a SFOPT is possible in the present scenario, as we will show explicitly in Sect. 5. Finally, we stress that the heavy neutrinos produced in the decays of the 125 GeV Higgs bosons may themselves decay visibly inside the detector via active-heavy neutrino mixing, leaving a prompt or displaced vertex signal in the detector depending on the value of θ^2. In particular, if the heavy neutrinos N_i are long-lived, they can lead to a two-displaced-vertices signal in the LHC detectors, which would be a very powerful probe of the model [84,85].

3.3 Electroweak precision observables

The properties of the singlet field are also constrained by EW precision observables (EWPO), which limit the value of the mixing $\sin\xi$ as a function of the scalar mass M_S in the singlet scalar extension of the SM (see e.g. [86,87]). This is a result of the shift induced by the presence of the singlet scalar on the EW oblique parameters S, T, U[88] with respect to the SM. A global fit to EWPO measurements yields the respective values of the shifts on the oblique parameters with respect to their SM predictions [89]

$$S = 0.04 \pm 0.11,\ T = 0.09 \pm 0.14,$$
$$U = -0.02 \pm 0.11, \tag{3.11}$$

with the following correlation coefficients: $+0.92$ between S and T, -0.68 between S and U and -0.87 between T and U. Explicit expressions for S, T, U in the singlet scalar extension of the SM are given in [87] as a function of $\sin\xi$ and M_S. Using these, we obtain the 95% C.L. limits on the $(M_S, |\sin\xi|)$ plane from a χ^2 fit to the S, T, U measurements from Eq. (3.11). These are shown in Fig. 2, highlighting that for values of M_S below a TeV, the bound from Higgs signal strength discussed in the previous section is stronger than that of EWPO.

Notice, however, that the same EWPO used to constrain S, T and U and, from there, derive constraints on $\sin\xi$ are affected already at tree level and used to derive the bounds on the heavy-active neutrino mixing θ as outlined above [67]. In principle, the two contributions should be studied together to derive a consistent set of constraints. The interplay between new physics contributions to the EWPO through S, T, U and the presence of heavy neutrinos was studied in detail in Refs. [90–93]. In particular, it was realized that most observables depend on the same combination of elements of θ and T and that, if a cancellation between these two contributions is present, the bounds on both sources of new physics would weaken significantly. Nevertheless, for this situation to take place, negative and sizable values of T are required [93]. The scalar singlet contribution to T does indeed become negative for masses above the mass of the Higgs (see e.g. [87]). For lighter singlet masses, no cancellation is possible and the two effects would rather reinforce each other, leading to slightly stronger constraints. Nevertheless, since the bounds from Higgs signal strength are more stringent, the potential contribution of the singlet is small and does not alter significantly the constraints on heavy-active neutrino mixing derived in [93]. Conversely, for a scalar singlet heavier than the Higgs, the bound $\mathrm{tr}\left(\theta\theta^\dagger\right) \leq 0.0048$ would weaken if $-2\alpha T \sim 0.0048$. However, given the bounds on $\sin\xi$ from the LHC Higgs signal strength measurements (see Sect. 3.2), this is never achieved for sub-Planckian scalar masses. Thus, for the parameter space under study, the possible interplay between the heavy neutrino and scalar singlet contributions to EWPO can be safely neglected.

3.4 Searches for singlet-like scalars at LEP and LHC

Under the assumption that the singlet-like scalar decays into SM particles (i.e. its decay is driven by the singlet-doublet mixing), the null results from LEP searches for Higgs-like particles yield strong upper limits on $|\sin\xi|$ for singlet-like scalar masses below $M_S \simeq 115$ GeV (see e.g. [73]). These limits are at the level of $|\sin\xi| \lesssim 0.2$ (or below) for masses $M_S < 100$ GeV. At the same time, LHC searches for BSM scalars decaying to WW, ZZ or HH pairs also constrain the doublet admixture of the singlet-like scalar S for $M_S > M_H$. For $M_S > 200$ GeV the strongest such limits are obtained by ATLAS in the $ZZ \to 4\ell$ and $ZZ \to 2\ell 2\nu$ final states [83].[9] In Fig. 2 we show the corresponding bounds on the $(M_S, |\sin\xi|)$ plane from both LEP and LHC searches for new scalars, under the assumption $\mathrm{BR}_{S\to HH} + \mathrm{BR}_{S\to \mathrm{BSM}} \equiv \mathrm{BR}_{H+X} = 0$ (dashed lines).

Nevertheless, compared to the minimal singlet extension of the SM, here the presence of the heavy neutrinos may lead to much less stringent bounds on $\sin\xi$ from direct scalar

[8] Writing $\mathcal{Y}_N^2 = R\,(M_H/2\,\omega_{EW})^2$ (with $R > 1$), for $R/n > 1$ the Higgs decay into at least one heavy neutrino N_i must be kinematically forbidden, while for $R/n < 1$ it is still possible to have $k = n$ in Eq. (3.9).

[9] For masses $M_H < M_S < 200$ GeV, only $\sqrt{s} = 7$ and 8 TeV LHC limits exist [94,95]. These are not competitive with present Higgs signal strength bounds on $\sin\xi$, and we disregard them.

searches. Indeed, the interactions of S with the heavy neutrinos N_i in Eq. (3.7) will induce the decay $S \to N_i \bar{N}_i$ if available by phase space. The corresponding partial width $\Gamma^S_{N\bar{N}} \propto \cos^2\xi$, in contrast to the partial decay widths of S into SM states, $\Gamma^S_{\rm SM} \propto \sin^2\xi$. Thus, $S \to N_i \bar{N}_i$ will generally be the dominant decay channel for the singlet-like scalar in the limit $|\sin\xi| \ll 1$ (as favoured by LHC Higgs signal strength measurements, see Sect. 3.2):

- For light singlets ($M_S \lesssim 100$ GeV), the $S \to N_i \bar{N}_i$ decay channel would significantly relax constraints on $\sin\xi$ from LEP searches for Higgs bosons decaying visibly (into SM particles), and we show the corresponding dilution of the limits when $\text{BR}_X = \text{BR}_{S\to N_i\bar{N}_i} = 0.9$ in Fig. 2. Nonetheless, if the heavy neutrinos N_i are long-lived (e.g. for very small neutrino mixing) and would have escaped the LEP detectors, limits from LEP searches for invisibly decaying Higgses [96–99] would apply. We also depict the bounds from such searches on $\sin\xi$ in Fig. 2, showing that they become very strong for rather light scalars. We nevertheless re-stress that these only apply under specific conditions (very long-lived N_i, leading to invisible S decays), which depend on the details of the neutrino sector of the model.
- For $M_S \gtrsim 200$ GeV, the presence of the $S \to N_i \bar{N}_i$ decay would weaken the LHC limits on $\sin\xi$ from $pp \to S \to ZZ$ searches, as shown explicitly in Fig. 2 for $\text{BR}_{H+X} = 0.9$.[10] At the same time, this BSM decay would open a new avenue to probe the existence of S and N_i at the LHC, either when the N_i decay products are resolved in the ATLAS/CMS detector or merge into a single reconstructed object (for $M_S \gg M_{N_i}$, producing a "neutrino jet" [103,104]). Yet, current LHC searches for heavy neutrinos generally consider N_i production modes (e.g. Drell–Yan or $W\gamma$ fusion, see [105] for a discussion) which yield kinematic properties of the N_i rather different from those of $S \to N_i \bar{N}_i$ decays,[11] and as such present LHC limits (see [107,108] for reviews) are difficult to extrapolate to our scenario. Moreover, the possibility that the N_i yield displaced decays (for $\theta^2 \ll 1$) would dramatically reduce the sensitivity of those existing searches, providing at the same time a new avenue for discovery in long-lived particle searches to be explored in the future.

3.5 Higgs self-coupling

Finally, the existence of the singlet scalar would induce a deviation on the Higgs boson trilinear self-coupling λ_{HHH} from its SM value. This is currently being searched for at the LHC [109–111] via non-resonant di-Higgs production, albeit with limited precision at present. At tree-level, we find

$$\lambda_{HHH} = \lambda_h\, v_{EW}\, c_\xi^3 - \frac{2\,\lambda_m\,\omega_{EW} + \mu_m}{4} c_\xi^2 s_\xi + \frac{\lambda_m\, v_{EW}}{2} c_\xi s_\xi^2 - \frac{3\,\lambda_s\,\omega_{EW} + \mu_3}{3} s_\xi^3, \tag{3.12}$$

with $\cos\xi\,(\sin\xi) = c_\xi\,(s_\xi)$. Additionally, and particularly relevant in the $|\sin\xi| \ll 1$ limit, the one-loop corrections to the trilinear self-coupling coupling should be taken into account, as they contain terms that do not vanish even when $\sin\xi \to 0$. The one-loop contribution reads, in the $|\sin\xi| \ll 1$ limit [17]

$$\Delta\lambda^{1-\text{loop}}_{HHH} = \frac{1}{16\pi^2}\left(\lambda_m^3 \frac{v_{EW}^3}{2\,M_S^2} + 27\frac{M_H^4}{v_{EW}^3} + 3\lambda_m^2 \frac{\mu_3\, v_{EW}^2}{M_S^2} s_\xi\right). \tag{3.13}$$

We parametrize the deviation with respect to the SM as

$$\kappa_\lambda \equiv \frac{\lambda_{HHH} + \Delta\lambda^{1-\text{loop}}_{HHH}}{\lambda^{SM}_{HHH}}, \tag{3.14}$$

with $\lambda^{SM}_{HHH} = M_H^2/(2v_{EW})$ the tree-level value of the SM Higgs boson self-coupling.[12] The most stringent constraint on κ_λ has been recently set by the ATLAS Collaboration [111] to be

$$-1.0 \le \kappa_\lambda \le 6.6 \quad (95\%\,\text{C.L.}). \tag{3.15}$$

We note that the measurements of λ_{HHH} at the LHC via non-resonant di-Higgs production can be significantly altered by the presence of a resonant contribution to the di-Higgs signature (see [113,114] for a discussion), appearing in the singlet scalar extension of the SM via the $pp \to S \to HH$ process. Still, depending on the singlet-like scalar mass M_S, it should be possible to exploit the di-Higgs invariant mass distribution m_{HH} to measure the self-coupling λ_{HHH} [113] from the non-resonant part of the distribution (with the resonant part properly identified and subtracted), achieving comparable precision to the scenario with no resonant $S \to HH$ contribution. A detailed analysis of this issue is however beyond

[10] The presence of a non-zero $S \to HH$ partial width Γ^S_{HH} would also weaken the limits on $\sin\xi$ from $pp \to S \to ZZ$ searches, allowing at the same time to search for S via resonant di-Higgs production (see e.g. [100,101]). Yet, di-Higgs searches are generally less sensitive than ZZ ones for equal branching fractions, and the equivalence theorem [102] naively yields $\Gamma^S_{HH} \sim \Gamma^S_{ZZ}$ in the $M_S \gg v$ limit (since also $\Gamma^S_{HH} \propto \sin^2\xi$). We have thus not considered here the would-be limits from resonant di-Higgs searches for $\Gamma^S_{HH} \neq 0$ for simplicity.

[11] An exception is given by LHC searches for Z' gauge bosons decaying to heavy neutrinos [106], which feature similar kinematics and could allow for a reinterpretation in our setup. We defer this for future work.

[12] We remark that our definition of κ_λ matches that of the ATLAS and CMS experimental collaborations, yet $\kappa_\lambda = 1$ corresponds to the SM prediction only if one-loop corrections to λ_{HHH} in the SM (which amount to 9% of the tree-level value [112]) are neglected.

the scope of the present work. Moreover, as we will see in Sect. 5 this observable barely deviates from its SM value in the interesting regions of the parameter space and is therefore not a relevant probe of the scenario under study.

4 Parameter scan

In this section we describe our procedure to scan the parameter space of the model and collect the sets of parameters which fulfill the various necessary conditions for a SFOPT. As described in Sect. 2, in general a potential characterized by a random set of parameters $\{\omega, \omega_p, v, m_h^2, m_s^2, \lambda_m, T_c, \mathcal{Y}_v, \mathcal{Y}_N\}$ at $T = T_c$ will not yield the correct values of the Higgs vev and Higgs mass at $T = 0$, namely $v_{EW} = v_{EW}^{\rm exp} \equiv 246.22$ GeV and $M_H = M_H^{\rm exp} \equiv 125.10$ GeV. The first condition $v_{EW} = 246.22$ GeV can always be imposed starting from any given set of parameters by shifting all the parameters η with dimension of mass (including T_c) as $\eta \to (v_{EW}^{\rm exp}/v_{EW})\,\eta$. To satisfy the second condition, $M_H = M_H^{\rm exp}$, we solve for m_h^2 for each generated set $\vec{w} = \{\omega, \omega_p, v, m_s^2, \lambda_m, T_c, \mathcal{Y}_v, \mathcal{Y}_N\}$ to find values which reproduce the correct Higgs boson mass: in practice, for a given set $\vec{w}$ we scan m_h^2 imposing $v_{EW}/M_H = v_{EW}^{\rm exp}/M_H^{\rm exp}$ before the aforementioned shift of the mass dimensionful parameters η, which guarantees $M_H = M_H^{\rm exp}$ after it. A solution does not always exist depending on the actual values of $\vec{w}$. In this way, we obtain the sets of parameters which have two degenerate minima at $T = T_c$ and also reproduce the correct Higgs vev and mass at $T = 0$.

Following Ref. [15], we bias our scan towards the parameter sets that satisfy the necessary conditions for a SFOPT.[13] For this purpose, we have defined an ad-hoc weight function to rate how well the selected points satisfy these conditions, in order to prioritize the parameter regions to which the points belong in our scan. We then use this weight function in place of the log-likelihood for a Markov Chain MonteCarlo (MCMC) using the standard Metropolis Hastings algorithm to sample the interesting regions of the parameter space with MonteCUBES [115]. The conditions for a SFOPT and the weight function used in the MCMC are explicitly defined in Appendix A. Our procedure of the parameter scan is summarized in Fig. 3.

Finally, we have verified the validity of the high-T approximation adopted in Sect. 2 through a comparison of the value of T_c obtained in this approximation with the one obtained from a potential with the same parameters at $T = 0$ but implementing the temperature evolution with the full 1-loop thermal potential (see e.g. [116]). The comparison has been performed for points passing all viability criteria, as discussed below. Both values of T_c agree within 5% accuracy for the vast majority of the points scanned (a few outliers extend to $\sim$ 10%). Then, even though in some cases the value for the scalar singlet mass M_S found in the scan is of the same order as T_c, the high-T approximation can remain suitable for our purposes (a fast efficient scan of the parameter space). In addition, we impose a stringent perturbativity condition on the scalar quartic couplings, $\lambda_i \leq 2$ (see below), which favours that radiative corrections are not significant.

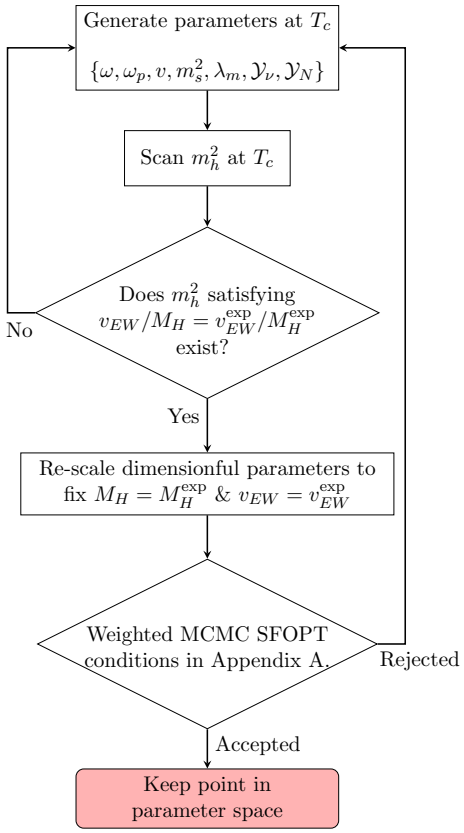

Fig. 3 Flowchart for the selection of parameter sets generating the correct Higgs vev and mass at $T = 0$ and satisfying all necessary conditions to potentially have a SFOPT from Ref. [15]

The parameter sets output of our MCMC scan are further classified according to the following viability criteria:

- Points with the scalar potential quartic couplings $\lambda_i \leq 2$ to ensure perturbativity.
- Points that lead to a sufficiently strong first-order phase transition (if the phase transition occurs). As a rough estimate, we ask for the ratio $v/T_c > 1$.
  This is required to make EW baryogenesis possible by decoupling sphaleron processes in the EW broken phase.
- Points for which the bubbles of the EW broken phase can actually nucleate and the phase transition does take place.

[13] Among the different conditions, we look for potentials that are bounded from below for which the EW minimum is the global one. While the EW minimum could be metastable, such setups are beyond the scope of this work.

Although the conditions summarized in Fig. 3 are needed to realize a SFOPT, they are not sufficient to guarantee it. It is important to study whether a nucleation temperature $T_N < T_c$ exists for which the bubbles of the EW broken phase (the true vacuum for $T < T_c$) successfully grow [17,60,62,117,118] (and the Universe does not become trapped in the false vacuum). In our scan of parameters, we gauge the nucleation of EW bubbles as follows:

The transition probability from the false to the true vacuum is proportional to $e^{-S_3/T}$, with S_3 the three-dimensional bounce action.

At temperatures slightly below T_c, in the so-called thin-wall regime for which the two minima are almost degenerate, the action S_3 diverges for $T \to T_c$ [119,120] and thus no transition is possible in this regime. As the Universe cools down from T_c to the nucleation temperature T_N, away from the thin-wall limit, the computation of the bounce action becomes more involved. It requires to solve the equations of motion for the background fields to find the bounce solution. This is usually done via numerical solvers like `CosmoTransitions` [121], `BubbleProfiler` [122] or `FindBounce` [123]. Nucleation will be possible if there exists a temperature $T_N > 0$ at which $S_3/T_N \sim 140$ [124–127], for which the nucleation rate is comparable to the Hubble expansion rate during radiation domination.

In order to estimate the bounce action and thus the nucleation temperature T_N, instead of computing the bounce solution along the path that minimizes the tunneling action, we approximate the solution by calculating the bounce action along a straight path in field space, which connects both minima at T_N. The action for such a field configuration, $S_3^{\rm app}$, will by construction be larger than the tunneling solution [128–130], $S_3 \leq S_3^{\rm app}$. We find that there is good agreement between the true action S_3 and our estimation for the cases of interest, and thus successful nucleation for points in parameter space is expected to occur when $S_3^{\rm app}/T_N \lesssim 140$, which in turn represents a conservative estimate. In practice, we rewrite the scalar potential in terms of a linear combination of h and s along the straight line connecting the minima at a given T, $\phi_\parallel$, and the orthogonal one, $\phi_\perp$, as prescribed in Ref. [131]. By taking $\phi_\perp \to 0$ one can quickly find the bounce solution along the straight line using the overshoot-undershoot method in one dimension with, for example, `FindBounce`. In this manner, the action $S_3^{\rm app}$ can be computed at the temperature T. The temperature at which $S_3^{\rm app}/T \sim 140$ defines the nucleation temperature T_N. As an example of our approximation, we compare in Fig. 4 the approximated and the actual bounce trajectories in field space with the set of parameters given in Table 1. This approximation allows us to efficiently scan the parameter space. In the results shown in the following section, the boundaries between the nucleating and non-nucleating points should therefore be understood as an approximated result and somewhat conservative. In Sect. 5 we will perform a comparison between the regions of parameter space selected by our nucleation criteria and those found using `CosmoTransitions`, finding good agreement between both methods.

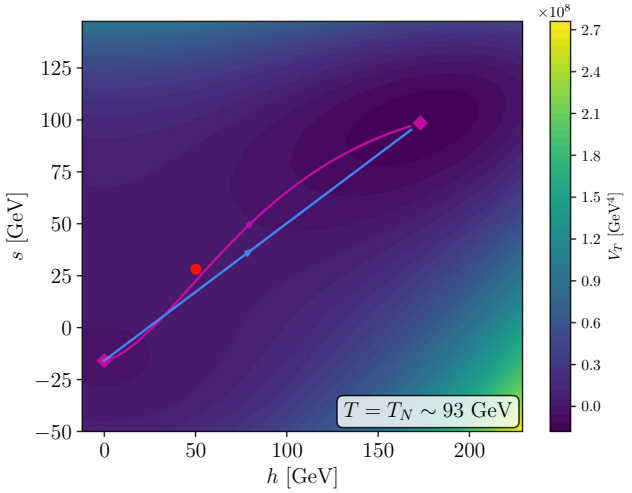

Fig. 4 The same as Fig. 1 but at the nucleation temperature T_N. The blue line corresponds to the straight path in the field configuration space which we use as an approximation to estimate the action and judge if nucleation may happen, while the purple curve corresponds to the actual bounce solution passing closer to the saddle point (red dot) between the two minima (purple diamonds)

- Points with the scalar mixing ξ at $T = 0$ allowed by collider searches as described in the previous section.

In the next section, we will show the impact of each of these conditions in the parameter space to reveal the correlations among the parameters and the preference for particular parameter regions. As we will see, the condition of the bubble nucleation will prove to be the most constraining one [17,60,62,118], which greatly reduces the allowed parameter space.

5 Results

In this section we present and analyze the results from the parameter scan described in Sect. 4 where the different constraints and conditions described in the previous section have been implemented. While the scan is performed over all parameters (at $T = T_c$) in $\vec{w} = \{\omega, \omega_p, v, m_s^2, \lambda_m, T_c, \mathcal{Y}_v, \mathcal{Y}_N\}$ with m_h^2 fixed so as to reproduce the correct Higgs mass, the constraint in the active-heavy neutrino mixing $\text{tr}\left(\theta\theta^\dagger\right)|_{\rm exp} \leq 0.0048$ [67] implies $\mathcal{Y}_v^2$ will have a negligible impact on the scalar potential. We will therefore not show this parameter in the follow-

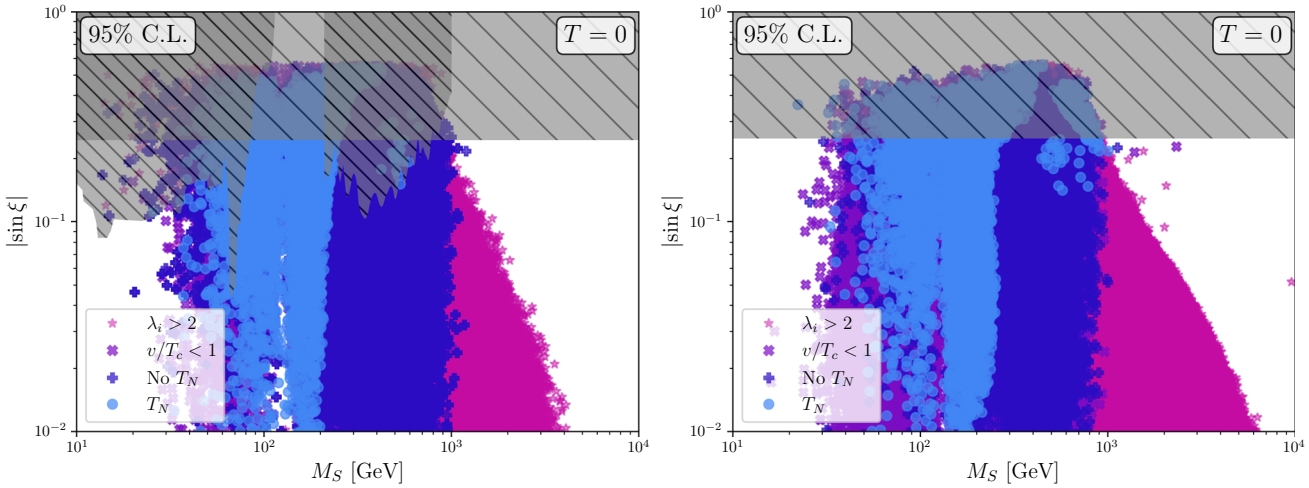

Fig. 5 Results of the parameter scan in the scalar mass, M_S, and mixing, $\sin\xi$, plane. In the right (left) panel the scan was performed with(out) the addition of the heavy Dirac neutrinos. The pink stars correspond to points with non-perturbative couplings, the purple crosses to points for which sphaleron transitions would not decouple in the broken phase. The light blue dots (dark blue pluses) additionally do (not) satisfy the nucleation condition as described in the text. The grey-shaded region corresponds to the bounds on the scalar mixing described in Sect. 3. In the right panel, we do not show the bounds that depend on the parameters in each point

ing. Instead we will mainly focus on parameters which have a direct connection to experimental observables, and thus refer the reader to Figs. 9 and 10 in Sect. 6 for results on the complete set of parameters at T_c, $\{\vec{w}, m_h^2\}$, and $T = 0$ respectively, as a summary of our results.

In Fig. 5 we show the points collected in our parameter scan in the plane of the mass and mixing of the scalar singlet (M_S, $|\sin\xi|$). We study and compare the scenarios with(out) the addition of the heavy Dirac neutrinos in the right (left) panels. All the points have been selected according to the algorithm summarized in Fig. 3 and, therefore, satisfy the conditions from Ref. [15] for a SFOPT and have the correct Higgs mass and vev at $T = 0$. The points with different colours and symbols are classified by the conditions listed in Sect. 4. The pink stars are discarded since they have at least one very large scalar coupling ($\lambda_i > 2$).[14] For the purple crosses, this perturbativity condition is satisfied, but the first-order phase transition is not strong enough to decouple the sphaleron process in the EW broken phase ($v/T_c < 1$), even if the bubbles of the broken phase may nucleate. The dark blue crosses labeled with "No T_N" have $\lambda_i < 2$ and $v/T_c > 1$ but the nucleation condition $S_3^{\rm app}/T \lesssim 140$ is not satisfied at any $T < T_c$ (and therefore, there is no T_N). Finally, the light blue dots labeled with "T_N" have $\lambda_i < 2$ and $v/T_c > 1$ and also fulfill the nucleation condition. Grey-shaded areas in the left panel represent the values of the scalar mixing ruled out by LHC Higgs signal strength measurements (assuming $\mathrm{BR}_X = 0$) as described in Sect. 3.2, or by direct searches for Higgs-like particles at LEP for $M_S \lesssim 100$ GeV and at ATLAS for $M_S > 200$ GeV (assuming $\mathrm{BR}_{S\to HH} = 0$). On the right panel we only display the conservative Higgs signal strength bound in the absence of exotic Higgs decays, since the bounds from direct scalar searches at LEP and LHC may be diluted when heavy Dirac neutrinos are included, depending on the values of neutrino couplings as discussed in Sect. 3.4. As can be seen from the plots, these constraints are quite relevant and a big portion of the parameter space is ruled out by them, so that only small values of $\sin\xi$ are still allowed. Moreover, we also find that the condition of successful bubble nucleation considerably reduces the size of the viable parameter space, as pointed out in Refs. [117,118] for other scenarios. Thus, only the light blue dots below the grey-shaded regions are successful candidates for a SFOPT satisfying all phenomenological constraints listed in the previous section. From Fig. 5 we can also see that the Universe may undergo an EW SFOPT only if the mass of the singlet scalar S is $M_S \lesssim 300$ GeV. Generally speaking, higher values of M_S would also imply larger ω and hence a significant distance between the two minima, in general too large to allow for bubble nucleation. The apparent exception to this rule by the few points clustered around $M_S \sim 500-1000$ GeV can be understood through a closer inspection of their thermal evolution. Indeed, in these cases we find a SFOPT only in the singlet direction at $T \gg \mathcal{O}(100)$ GeV. After this transition, both the Higgs and the singlet vevs roll towards their values at $T = 0$, v_{EW} and ω_{EW}, respectively, with $\omega_{EW} \gg v_{EW}$.

Through the comparison between the left and right panels of Fig. 5, we can study the impact of the presence of heavy Dirac neutrinos. While we find new nucleating regions char-

[14] Such large couplings will drive the model into a non-perturbative regime at scales very close to the EW scale, and thus we disregard those points in our scan.

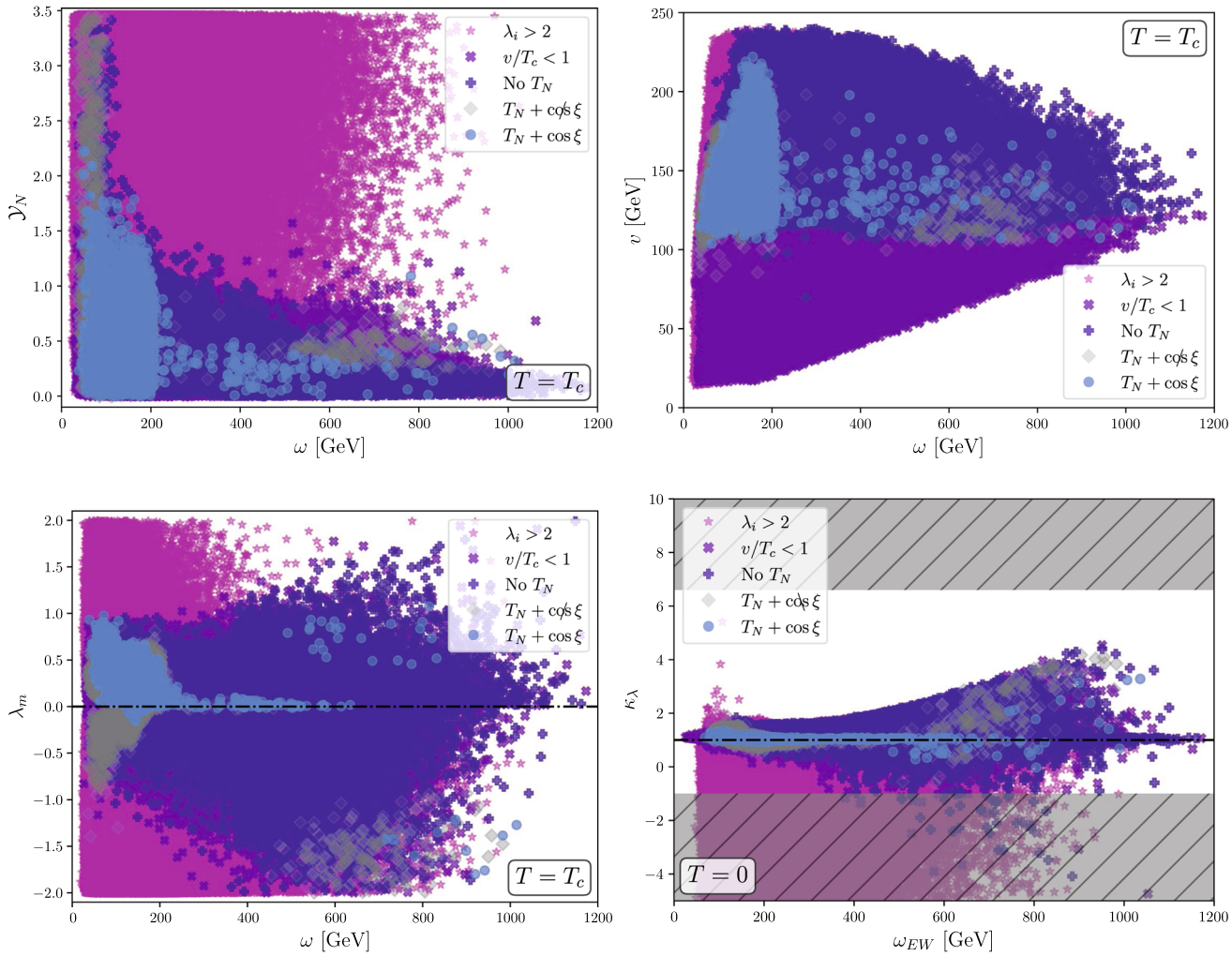

Fig. 6 Correlations between different parameters in the scan with non-zero neutrino Yukawa coupling. The allowed regions are very similar for the scan without neutrino Yukawas (see also Fig. 10). The color coding is the same as in Fig. 5 with the grey diamonds indicating the parameter space which can undergo successful nucleation but are excluded by their value of the scalar mixing ξ. In all panels the parameters are represented at $T = T_c$ except for the bottom-right panel with the trilinear Higgs coupling at $T = 0$

acterized by large ω and sizeable and negative λ_m (as can be seen in Fig. 10), these are largely ruled out by the constraints from Higgs signal strength measurements, as shown in Fig. 9. Indeed, as shown in the upper-left panel of Fig. 6, the points that pass the criteria for the case including the heavy neutrinos cluster at small values of $\mathcal{Y}_N$ or small ω. The condition that leads to the (hyperbola-like) correlation shown in this panel is the requirement of the stability of the EW broken minimum imposed in Eq. (A.3), in particular that $m_s^2 > 0$ at $T = 0$. Since $\mathcal{Y}_N$ induces a negative evolution of m_s^2 from T_c down to $T = 0$, values of $\mathcal{Y}_N > 1$ are constrained in the scan unless T_c is small and/or λ_m is negative to cancel its effect in Eq. (2.5). This can be seen explicitly in the corresponding panels of Fig. 9. Such a cancellation is however prevented by the bounds on the scalar mixing, as indicated by the grey points in Fig. 9. Thus, from now on, we will only present the results of our scan with $\mathcal{Y}_N \neq 0$, i.e. in the presence of heavy Dirac neutrinos. However, the allowed regions should also be considered generally valid for the $\mathcal{Y}_N = 0$ scenario without the heavy neutrinos, with the caveat that direct scalar searches at LEP and ATLAS further constrain the parameter space.

We present the distribution of scan points in various other interesting slices of the parameter space in Fig. 6. For information on the distributions under the other parameters of the scan, we refer the reader to Fig. 9. The color coding and symbols is the same as for Fig. 5, but in addition to them, we now have the grey diamonds (labeled with "$T_N + \cos\xi$") indicating the parameter space points which can undergo successful nucleation but are excluded by their value of the scalar mixing $\sin\xi$. They correspond to the blue dots covered by the grey-shaded area in the right panel of Fig. 5. In the upper right panel of Fig. 6 we show the correlations found in our scan between the two scalar vevs at $T = T_c$. As can be seen, the

most significant constraint is the requirement of a sufficiently strong EW phase transition, $v/T_c > 1$. When imposing this together with $v_{EW} = v_{EW}^{\rm exp}$ and $M_H = M_H^{\rm exp}$, values of v below ~ 100 GeV are ruled out. Besides this constraint, we find that large values of ω, beyond ~ 200 GeV, are disfavored by the requirement of successful nucleation. Indeed, we generally find that, if ω were too large, the field distance between the two minima would be too big to allow for bubble nucleation despite satisfying the rest of the requirements. Even though we find regions of parameter space successfully nucleating for singlet vevs as large as $\omega \sim 1000$ GeV at T_c, a detailed study of these regions shows that these transitions at T_N occur from $(0, \omega - \Delta\omega) \to (0, \omega)$, with $\Delta\omega \ll \omega$, such as the distance travelled in field space is not qualitatively larger than for the region with $\omega \lesssim 200$ GeV.

In the lower left panel of Fig. 6 we show the distribution of scan points in the $\omega - \lambda_m$ plane at $T = T_c$. We find that the light-blue dots, which pass all requirements and in particular the nucleation condition, display an anticorrelation between these two parameters. Additionally, the bounds on $\sin\xi$ rule out most of the points with $\lambda_m < 0$ unless $|\lambda_m| \ll 1$. These trends can be understood from the hyperbolic shape of the correlation between λ_m and ω_p, which is found in the corresponding panel of Fig. 9. Indeed, from Eq. (2.9) this behavior is expected if μ_m is negative. Analyzing the accepted samples, we find that negative μ_m is preferred in order to satisfy our condition for successful nucleation. In fact, negative μ_m decreases the barrier between the two degenerate minima and thus we find no nucleating samples for positive μ_m. Finally, the area with negative $\lambda_m < 0$ and negative ω_p is ruled out by the constraints on the scalar singlet mixing since, as expected from Eq. (2.9), $-m_{sh}^2$ would become too large.

We have further analyzed the non-trivial correlation found between ω and λ_m when imposing our criteria for nucleation, comparing these results with points that successfully nucleate according to the *tunneling module* from `CosmoTransitions`. As can be seen in Fig. 7, for a subset of our sample featuring successful nucleation, the areas found by both our approximate estimate (light-blue points) and `CosmoTransitions` (black octagons for a first-order EW phase transition) generally agree well. The two exceptions we identify are: (i) the region with negative λ_m and large ω, where `CosmoTransitions` finds successfully tunneling points which are not found by our approximation.[15] This region corresponds to significantly more curved trajectories

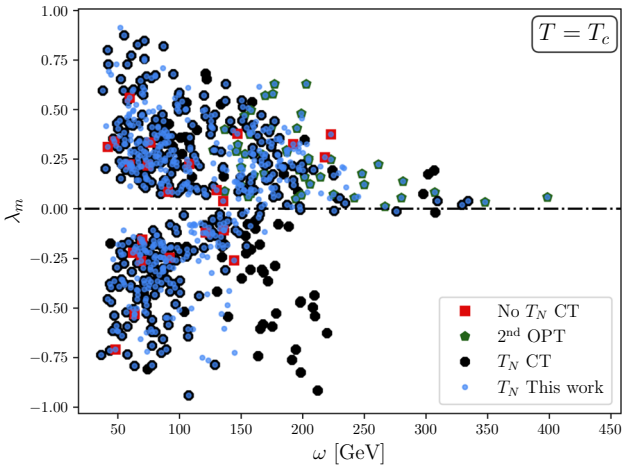

Fig. 7 Sample comparison between the results obtained with our proxy (light blue circles) and `CosmoTransitions` (CT) in the $\omega - \lambda_m$ plane for successfully nucleating points. According to CT, red squares correspond to non-nucleating points, green pentagons to those giving a 2nd order phase transition (OPT) and black octagons to successfully nucleating points

than those depicted in Fig. 4, not-well approximated by our straight-line assumption. Nevertheless, this whole area of the parameter space also leads to too large scalar singlet-doublet mixing (as described above) and is experimentally excluded. (ii) The points for which `CosmoTransitions` does not find an EW phase transition, whereas our nucleation proxy does, i.e. the red squares and the blue points with no counterpart (neither red square, green pentagon or black octagon) in Fig. 7. This should a priori never happen, since our criterium for nucleation is conservative. A careful investigation of such points reveals that the *p*hase-tracking module of `CosmoTransitions` does not produce numerically reliable results in such cases.[16] We thus conclude that neither of these exceptions is meaningful, and our estimate for nucleation agrees well with the results from `CosmoTransitions` for the values of the parameters for which `CosmoTransitions` yields a reliable numerical result, thus representing an efficient and fast alternative for scans of the parameter space discriminating in a conservative way if nucleation could happen.

As discussed in Sect. 3, the inclusion of the singlet scalar causes a deviation of the Higgs trilinear coupling from its SM value, which can be parametrized as in Eq. (3.14). The distributions of κ_λ as a function of ω_{EW} at $T = 0$ is shown

[15] For positive λ_m and large ω, a few of the light-blue points yielding successful nucleation with our criteria are instead tagged as second-order phase transitions (2ndOPT, green pentagons) by `CosmoTransitions` While we have not explicitly discerned the order of the transition in our scan (which is beyond our present scope), we note that no qualitative new regions appear when considering such parameter points, as this region falls within the areas where a SFOPT is found by our method.

[16] Even if by construction two phases are always present for our model parameter points, in these cases `CosmoTransitions` fails to find one of them for the default numerical precision in the code. A significant increase in the numerical precision generally leads to `CosmoTransitions` finding the second phase and identifying a first-order transition, in agreement with our estimate. Nevertheless, this increase in numerical precision makes the computation too slow to allow for an efficient scan of the parameter space.

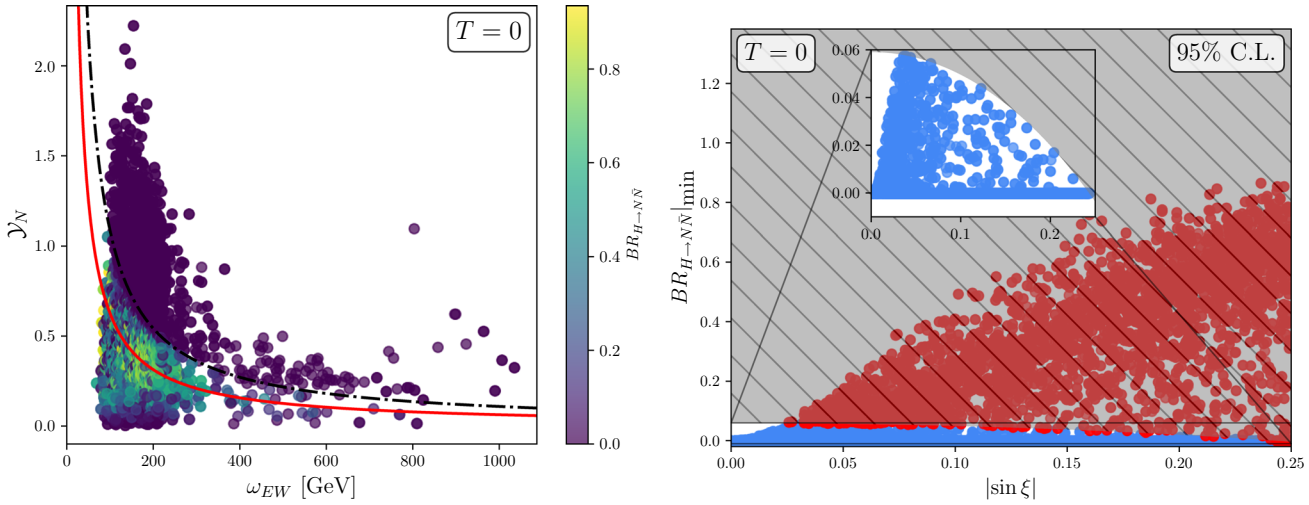

Fig. 8 Bounds on the regions of parameter space giving rise to successful nucleation. The left panel correspond to the plane $\mathcal{Y}_N$ against ω_{EW} at $T = 0$, with the color legend giving the size of $\mathrm{BR}_{H\to N\bar{N}}$ for $n = 3$ degenerate heavy neutrinos. The solid red line corresponding to $\omega_{EW}\mathcal{Y}_N = (M_H/2)$ separates the cases where the decay is always allowed (below) and where it depends strongly on the assumptions on the neutrino Yukawas Y_{N_i} (above). The dashed black line yields the boundary of kinematically allowed $H \to N_i\bar{N}_i$ decay for the $n = 3$ degenerate neutrino case. The right panel shows the excluded parameter space at 95% C.L. from Higgs signal strength measurements, in which red points are excluded while blue ones comply with the bounds, and is independent of n

in the bottom-right panel of Fig. 6, together with the current bounds from collider searches, which are given by Eq. (3.15) and shown by the grey-shaded regions. We find that the light-blue points satisfying all conditions tend to cluster in a narrow range around $\kappa_\lambda \sim 1$. Thus, given the sensitivity to $\kappa_\lambda \sim 2.2$ [132] of future probes such as the HL-LHC, no deviations caused by a singlet scalar responsible for a SFOPT are to be expected in this observable.

Finally, in Fig. 8 we show the regions of the parameter space which are constrained by the possible new decay channel of the Higgs-like state H into heavy neutrinos using Eqs. (3.8) and (3.9) as described in Sect. 3.2, for points which pass all the constraints (i.e. light-blue in Fig. 6) in our parameter scan. In the left panel we show the contribution to the corresponding branching ratio assuming a degenerate heavy neutrino spectrum ($Y^2_{N_i} = \mathcal{Y}^2_N/n$) with $n = 3$, for which $\Gamma_{H\to N\bar{N}}$ can be comparable to or even exceed the SM Higgs boson total width Γ_{SM} in an important part of the parameter space. The solid red line separates "Case 1" and "Case 2" as discussed in Sect. 3.2. Note that in the region above the solid red line ("Case 2"), a different combination of Y_{N_i} Yukawa couplings (yielding the same value of $\mathcal{Y}^2_N$) could arbitrarily reduce the value of $\mathrm{BR}_{H\to N\bar{N}}$ by making all neutrinos either too heavy for the Higgs to decay into or with negligible couplings. From this panel we can also infer that the heavy Dirac neutrinos are in general lighter than ~ 300 GeV. In the right panel of Fig. 8 we instead show the minimum possible value of $\mathrm{BR}_{H\to N\bar{N}}$ for each parameter point. Notice that for the points corresponding to "Case 1" (region below the solid red line in the left panel) the exclusion limits from Higgs signal strength measurements, shown in grey, are unavoidable and rule out a significant region of the parameter space, while for "Case 2" the $\mathrm{BR}_{H\to N\bar{N}}$ can be made arbitrarily small and thus the bound can always be evaded. In Fig. 9 we show in red the points excluded by $BR_{H\to N\bar{N}}$ in the different relevant planes in parameter space. Even though these constraints are important, as seen in Fig. 8, they do not exclude particular regions of parameter space.

6 Summary and conclusions

In this work we have explored the parameter space of the scalar singlet extension of the SM with the aim of identifying the regions in which a SFOPT, as required to explain the puzzle to the origin of the observed baryon asymmetry through the EWBG mechanism, can take place. The main goal of the study is to contribute to the predictability of the scenario by relating the areas where a SFOPT can happen with potentially testable observables or correlations among them.

Previous studies [15] showed the conditions that need to be met by the extended scalar potential in order to develop two degenerate minima at some critical temperature T_c. Together with the requirement of reproducing the correct mass and vacuum expectation value of the SM-like Higgs and of the required strength of the transition ($v/T_c > 1$), these set of constraints already impose stringent and non-trivial conditions of the allowed parameter space.

Nevertheless, as advocated by [17,60,62,117,118], we find that the requirement that bubble nucleation may actually take place between the two minima is the most constraining requirement, reducing drastically the allowed parameter space. Furthermore, testing explicitly this condition is not possible in a fast and analytical way and relying on the numerical solvers available [121–123] necessarily limits the speed of the scan hindering the exploration of large parameter spaces. Moreover, given the complexity of the problem, for some points in the parameter space we find that some numerical solvers fail to find one of the phases, and hence the corresponding transition, or are unable to produce a result. For this reason we have adopted a fast and conservative approximation to the three-dimensional action of the bounce solution, S_3^{app}, that controls the transition rate between the two minima and requires $S_3^{\text{app}}/T_N \sim 140$ at some nucleation temperature T_N. We find that for most of the sampled points in the parameter space that satisfy this criteria, `CosmoTransitions` does indeed find a first order phase transition (with a small fraction of second order transitions, something we did not explicitly discriminate), thus validating our approach. We also point out that, for many of the points that passed our selection criteria, `CosmoTransitions` did not provide an output. Thus, larger regions of the parameter space may be explored in a fast and efficient way through the approximation adopted, although it should be taken as a conservative estimate and not as an exact result.

In our scan of the parameter space we find that the regions with the correct mass and vev for the Higgs and successful nucleation are mainly characterized by values of the singlet vev $\omega_{EW} \lesssim 300$ GeV. Indeed, if ω_{EW} is too large, the two minima tend to be too far apart in field space[17] and nucleation may not happen. This in turn translates into values of the scalar singlet mass that cluster around $M_S \lesssim 300$ GeV. The exception to this rule is a clustering of allowed points with large ω and values of M_S in the 500–1000 GeV range, which in any case do not produce an EW phase transition given that $v(T)$ smoothly goes from 0 to v_{EW} as the Universe expands. We have verified that for these points the actual jump in ω during the phase transition is also small. Regarding the most constraining observables, we find that the bounds on the singlet-doublet mixing from Higgs signal strength measurements by ATLAS and CMS are already ruling out important regions of the parameter space. Direct searches for the singlet scalar when its decays are SM Higgs-like both at LEP and at LHC are also relevant.

We have also investigated how this picture is affected when the scalar singlet is not alone, but part of larger dark sector it may interact with. As a particularly motivated scenario, we considered as case study the addition of extra sterile neutrino singlets of both chiralities. These new states will have Yukawa couplings Y_N to the scalar singlet, which would induce Dirac masses around the EW scale for these heavy neutral leptons. Furthermore, a Yukawa coupling Y_ν among the SM Higgs doublet, the SM neutrinos and the heavy neutrinos would generally also be allowed. The simultaneous presence of Y_N and Y_ν implies a new source of CP-violation that may be enough to induce the BAU via EWBG [18,19] (the so-called ν-EWBG scenario [19]). Furthermore, if a small source of lepton-number violation is introduced, the presence of Y_ν would induce small neutrino masses able to explain the neutrino oscillation phenomenon in the manner of the low-scale symmetry-protected seesaws like the inverse or linear seesaw variants.

Previous studies [21] showed that the presence of the heavy neutrinos increases the strength of the transition by enhancing v/T_c. We reproduce this result, but find that sizable Y_N, unless accompanied by small ω, can also destabilize the broken minimum. Thus, when our criteria for nucleation and stability are imposed, for the allowed values of the Yukawa couplings the regions of the scalar potential parameter space are comparable to the scenario without heavy neutrinos. Hence the early universe phenomenology regarding the possibility of a SFOPT of both scenarios is very similar, as summarized in Figs. 9 and 10. Even if new areas appear when including the neutrinos, we observe in Fig. 9 that they are excluded by Higgs signal strength measurements. The small values of the Yukawa couplings and the scalar singlet vev ω preferred, seem to make the generation of the BAU via EWBG difficult according to the findings of [19], but a dedicated analysis would be required to confirm or rule out its viability.

Conversely, the presence of the heavy sterile neutrinos may significantly affect the collider phenomenology of the scalar singlet extension. Indeed, while very large values of Y_N could hinder vacuum stability, values around $Y_N \sim \mathcal{O}(1)$ are perfectly allowed. Such a sizable coupling would on the one hand imply that the scalar singlet decays would be overwhelmingly dominated to the heavy sterile neutrino channel, given that the singlet-doublet mixing is more strongly constrained and the smaller SM Yukawa couplings. This would in turn invalidate the bounds on the scalar mixing derived from direct searches of the singlet with SM-like decays at LEP and LHC. On the other hand, dedicated searches for this new decay channel should be considered.

Furthermore, if allowed by phase space, the decay to heavy sterile neutrinos could also be sizable for the SM-like Higgs scalar via its mixing with the singlet. We have found that this in fact strengthens the Higgs signal strength constraints in significant portions of the parameter space, correspond-

[17] Without loss of generality, exploiting the shift symmetry of the potential, we choose the value of the singlet vev at the EW symmetric minimum to also vanish at the critical temperature.

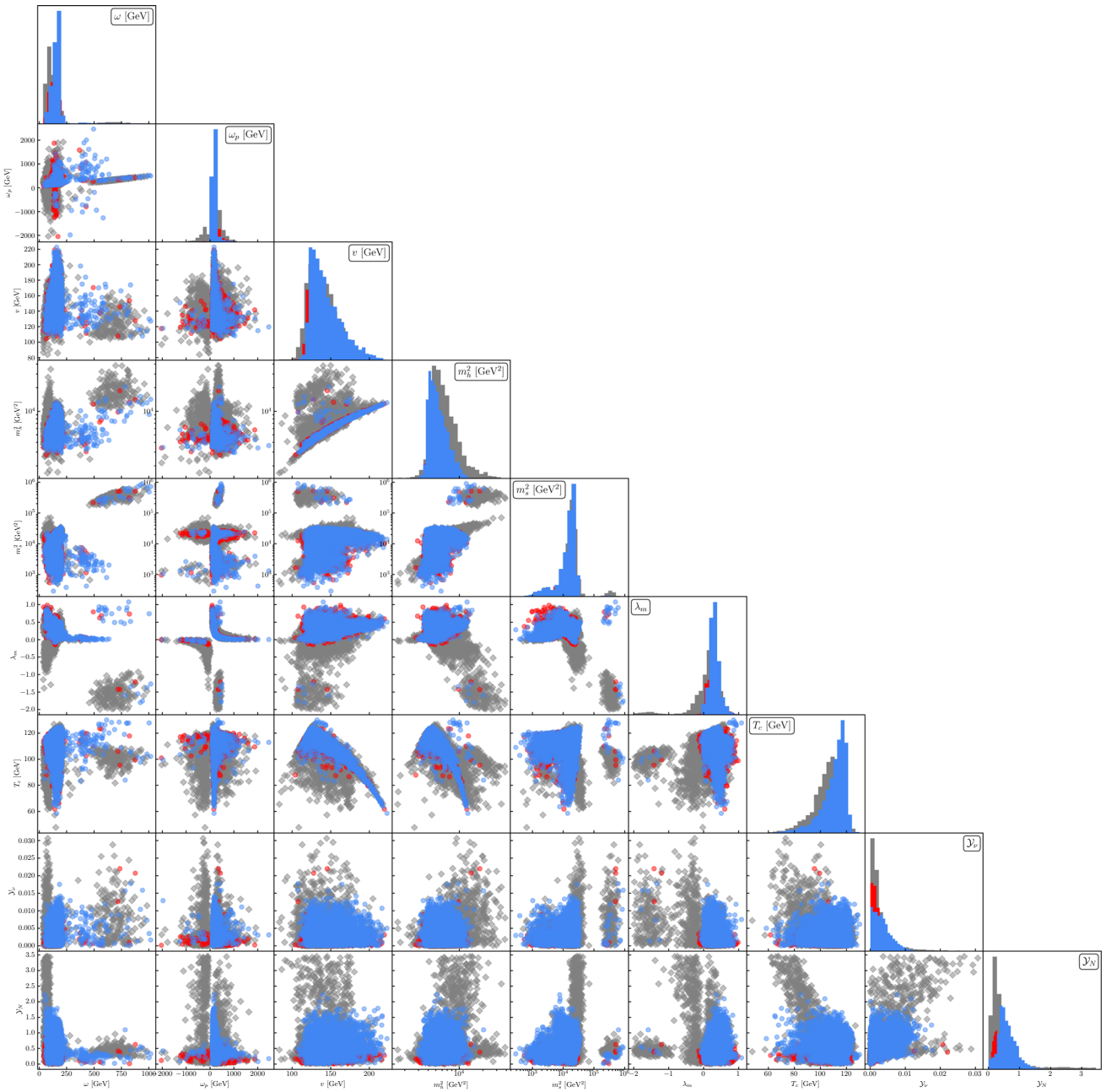

Fig. 9 Triangle plot for non-zero Yukawas, only for points successfully nucleating. The grey diamonds correspond to regions of parameter space excluded by constraints on the scalar mixing while red dots are excluded by the constraint from $H \to N\bar{N}$. The blue points satisfy all phenomenological bounds. We note the very strong correlation between the singlet vev ω and ω_p at T_c for blue points, as well as between λ_m and ω_p

ing to the red points in Fig. 8. Interestingly, the possibility that this is the dominant channel to produce and test for the heavy neutrinos at collider searches also remains open in parts of the parameter space. Indeed, the mixing of the heavy neutrinos with their active counterparts induced by Y_ν is more strongly constrained from flavour and electroweak precision observables, as well as collider searches via Drell–Yan production. Thus, if Y_N is more sizable than Y_ν, the heavy neutrinos would be more easily produced via Higgs or singlet decays. For small enough values of Y_ν, the decays of the heavy neutrinos themselves would not be prompt and may induce interesting signatures with displaced vertexes. We thus find that the viable parameter space allows for very striking and non-standard collider phenomenology

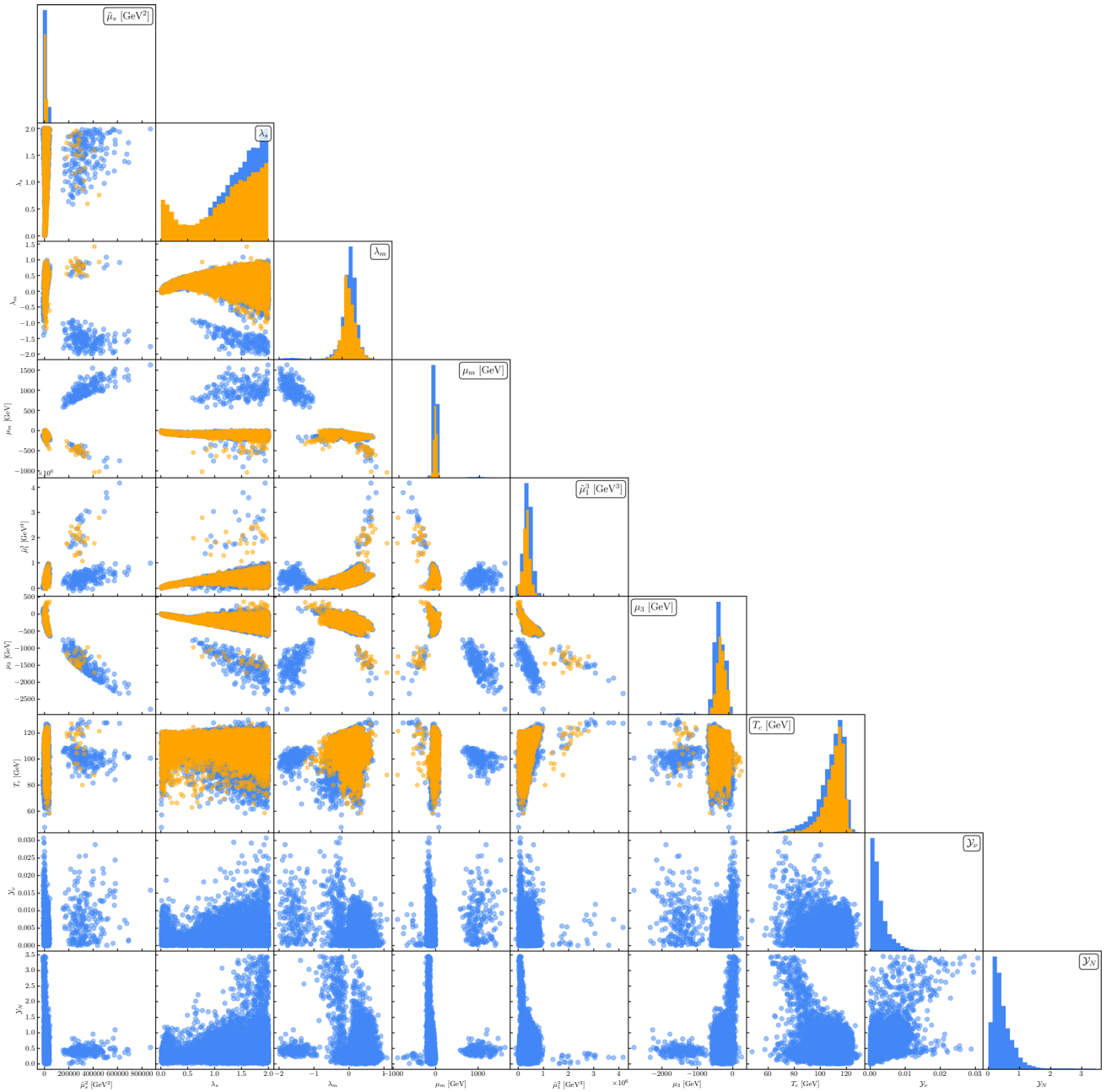

Fig. 10 Triangle plot comparing the successfully nucleating points for the singlet scalar alone (orange pentagons) and including the neutral fermions (blue dots), without imposing any phenomenological bound, at $T = 0$ for the parameters defined in Eq. (2.3). In the singlet-scalar-only case we have $\mathcal{Y}_{\nu(N)} = 0$ and it is not shown in the plot

which will be interesting to pursue in future dedicated studies.

Acknowledgements We acknowledge very helpful discussions with Josu Hernandez-Garcia and Daniel Naredo-Tuero. We also thank Jose Ramón Espinosa for invaluable discussions regarding tunneling. The work of J.M.N. was supported by the Ramón y Cajal Fellowship contract RYC-2017-22986, and by grant PGC2018-096646-A-I00 from the Spanish Proyectos de I+D de Generación de Conocimiento. E.F.M., J.M.N and T.O. acknowledge partial financial support by the Spanish Research Agency (Agencia Estatal de Investigación) through the grant IFT Centro de Excelencia Severo Ochoa No CEX2020-001007-S and (E.F.M and T.O.) by the grant PID2019-108892RB-I00 funded by MCIN/AEI/ 10.13039/501100011033. The authors also acknowledge support through the European Union's Horizon 2020 research and innovation programme under the Marie Sklodowska-Curie grant agreements No 860881-HIDDeN and No 101086085-ASYMMETRY. JLP also acknowledges support from Generalitat Valenciana through the plan GenT program (CIDEGENT/2018/019) and the Spanish Ministerio de Ciencia e Innovacion project PID2020-113644GB-I00.

Data Availability Statement This manuscript has no associated data or the data will not be deposited. [Authors' comment: As this is a theoretical study, no data were collected for our study.]

Funded by SCOAP[3]. SCOAP[3] supports the goals of the International Year of Basic Sciences for Sustainable Development.

A Parameter scan with weight function

We describe in this section the ad-hoc weight function used for the parameter scan and also show the distribution of the parameter points that satisfy the nucleation condition in the full parameter space at Fig. 9.

A set of necessary conditions for a successful SFOPT were identified, analytically, in Ref. [15], and can be found in Table 1 therein. They fall into the following three categories:

- Conditions to have degenerate minima at $T = T_c$:
  In order for the two minima to be stable we impose

$$\begin{aligned} &\det(\mathcal{M}_s) - \frac{v^2}{\omega^2}(m_h^2|_0)m_h^2 > 0, \\ &m_h^2|_0,\ m_h^2,\ m_s^2 > 0, \end{aligned} \tag{A.1}$$

  with $m_h^2|_0 \equiv (\omega/2)[\lambda_m - m_h^2/\omega^2 - 2m_{sh}^2/(v\omega)]$. These expressions are valid under the assumption that the symmetric minimum sits at $(0, 0)$, which we can assume without loss of generality thanks to the shift symmetry present in the potential.
- Matching conditions at T_c:
  Once a viable degenerate potential is found at T_c with the reduced set of parameters $\{\omega, \omega_p, v, m_h^2, m_s^2, \lambda_m\}$, we need to set the parameters λ^2, m_* (given by Eq. (2.8)) and m_{sh}^2 to particular values so as to have the general potential from Eq. (2.6). In this step we ensure that the running of the potential according to temperature change makes the broken minimum the deepest one by imposing

$$\left.\frac{d(V_{T,b} - V_{T,s})}{dT^2}\right|_{T_c} = c_h v^2 + \omega(c_s\omega + 2m_3) > 0, \tag{A.2}$$

  where $V_{T,b(s)}$ correspond to the potential in the broken (symmetric) minimum. Notice that in this step the neutrino Yukawa couplings $\mathcal{Y}_{\nu(N)}$ may play an important role as they enter into the c_h and c_s constants which set the running of the potential with the temperature.
- Conditions for potential at $T \leq T_c$:
  We require that the potential is bounded from below, and the broken minimum is the global minimum and stable, which are translated into the following conditions on the parameters at $T = 0$.

$$\begin{aligned} &\begin{cases} \lambda^2 > 0, & \text{for } \lambda_m \leq 0, \\ \lambda^2 + \frac{1}{4}\lambda_m^2 > 0, & \text{for } \lambda_m > 0, \end{cases} \\ &\det(\mathcal{M}_s^2),\ m_h^2,\ m_s^2 > 0, \\ &\lambda^2 - \frac{4m_*^2 v^2}{\det(\mathcal{M}_s^2)} \geq 0. \end{aligned} \tag{A.3}$$

  Notice that, as seems to be the case in the SM, the electroweak minimum could be metastable at $T = 0$ with a lifetime longer than the age of the Universe. Thus, this condition is more restrictive than strictly necessary. Nevertheless, it is convenient since it allows to efficiently scan the potential without the need of computing the lifetime of the vacuum.

All the conditions listed above take the form "$C_X > 0$" with C_X a given function of the parameters in the potential. In order to guide our scan towards the areas where these conditions are met we construct the following weight function

$$\mathcal{W} = \sum_X W_X, \tag{A.4}$$

with W_X defined as

$$W_X = \begin{cases} (10^6 C_X)^2, & \text{if } C_X \leq 0 \\ 0, & \text{if } C_X > 0. \end{cases} \tag{A.5}$$

The factor 10^6 is a penalty to the points that do not satisfy one of the conditions, with which we can make sure any point accepted in the MCMC satisfies all the necessary conditions for the SFOPT. We also add a Gaussian χ^2 term for the Higgs mass as well as for the constraint on $\mathcal{Y}_\nu$ from Eq. (3.3) as Gaussian priors to $\mathcal{W}$

$$\begin{aligned} \mathcal{W} = \sum_X W_X &+ \left(\frac{M_H - M_H^{\exp}}{\sigma_{M_H^{\exp}}}\right)^2 \\ &+ \left(\frac{\frac{n^2 v_{EW}^2}{2\omega_{EW}^2 \mathcal{Y}_N}\mathcal{Y}_\nu^2 - \mathrm{tr}\left(\theta\theta^\dagger\right)_{\exp}}{\sigma_{\mathrm{tr}(\theta\theta^\dagger)}}\right)^2, \end{aligned} \tag{A.6}$$

where $M_H^{\text{exp}} = 125.10$ GeV and $\sigma_{M_H^{\text{exp}}} = 0.17$ GeV is its uncertainty [64] and $\text{tr}\left(\theta\theta^\dagger\right)_{\text{exp}} = 0.0014$ with $\sigma_{\text{tr}(\theta\theta^\dagger)} = 0.0014$ [67,68], and we take $n = 3$.

References

1. A.D. Sakharov, Violation of CP invariance, C asymmetry, and baryon asymmetry of the universe. Pisma Zh. Eksp. Teor. Fiz. **5**, 32–35 (1967). https://doi.org/10.1070/PU1991v034n05ABEH002497
2. M.E. Shaposhnikov, Possible appearance of the baryon asymmetry of the universe in an electroweak theory. JETP Lett. **44**, 465–468 (1986)
3. M.E. Shaposhnikov, Baryon asymmetry of the universe in standard electroweak theory. Nucl. Phys. B **287**, 757–775 (1987). https://doi.org/10.1016/0550-3213(87)90127-1
4. A.G. Cohen, D.B. Kaplan, Thermodynamic generation of the baryon asymmetry. Phys. Lett. B **199**, 251–258 (1987). https://doi.org/10.1016/0370-2693(87)91369-4
5. A.G. Cohen, D.B. Kaplan, A.E. Nelson, Baryogenesis at the weak phase transition. Nucl. Phys. B **349**, 727–742 (1991). https://doi.org/10.1016/0550-3213(91)90395-E
6. A.G. Cohen, D.B. Kaplan, A.E. Nelson, Weak scale baryogenesis. Phys. Lett. B **245**, 561–564 (1990). https://doi.org/10.1016/0370-2693(90)90690-8
7. A.E. Nelson, D.B. Kaplan, A.G. Cohen, Why there is something rather than nothing: matter from weak interactions. Nucl. Phys. B **373**, 453–478 (1992). https://doi.org/10.1016/0550-3213(92)90440-M
8. M.B. Gavela, P. Hernandez, J. Orloff, O. Pene, Standard model CP violation and baryon asymmetry. Mod. Phys. Lett. A **9**, 795–810 (1994). https://doi.org/10.1142/S0217732394000629. arXiv:hep-ph/9312215
9. M.B. Gavela, M. Lozano, J. Orloff, O. Pene, Standard model CP violation and baryon asymmetry. Part 1: zero temperature. Nucl. Phys. B **430**, 345–381 (1994). https://doi.org/10.1016/0550-3213(94)00409-9. arXiv:hep-ph/9406288
10. M.B. Gavela, P. Hernandez, J. Orloff, O. Pene, C. Quimbay, Standard model CP violation and baryon asymmetry. Part 2: finite temperature. Nucl. Phys. B **430**, 382–426 (1994). https://doi.org/10.1016/0550-3213(94)00410-2. arXiv:hep-ph/9406289
11. K. Kajantie, M. Laine, K. Rummukainen, M.E. Shaposhnikov, Is there a hot electroweak phase transition at m(H) larger or equal to m(W)? Phys. Rev. Lett. **77**, 2887–2890 (1996). https://doi.org/10.1103/PhysRevLett.77.2887. arXiv:hep-ph/9605288
12. G. Degrassi, S. Di Vita, J. Elias-Miro, J.R. Espinosa, G.F. Giudice, G. Isidori et al., Higgs mass and vacuum stability in the Standard Model at NNLO. JHEP **08**, 098 (2012). https://doi.org/10.1007/JHEP08(2012)098. arXiv:1205.6497
13. J.R. Espinosa, M. Quiros, The electroweak phase transition with a singlet. Phys. Lett. B **305**, 98–105 (1993). https://doi.org/10.1016/0370-2693(93)91111-Y. arXiv:hep-ph/9301285
14. S. Profumo, M.J. Ramsey-Musolf, G. Shaughnessy, Singlet Higgs phenomenology and the electroweak phase transition. JHEP **08**, 010 (2007). https://doi.org/10.1088/1126-6708/2007/08/010. arXiv:0705.2425
15. J.R. Espinosa, T. Konstandin, F. Riva, Strong electroweak phase transitions in the standard model with a singlet. Nucl. Phys. B **854**, 592–630 (2012). https://doi.org/10.1016/j.nuclphysb.2011.09.010. arXiv:1107.5441
16. S. Profumo, M.J. Ramsey-Musolf, C.L. Wainwright, P. Winslow, Singlet-catalyzed electroweak phase transitions and precision Higgs boson studies. Phys. Rev. D **91**, 035018 (2015). https://doi.org/10.1103/PhysRevD.91.035018. arXiv:1407.5342
17. C.-Y. Chen, J. Kozaczuk, I.M. Lewis, Non-resonant collider signatures of a singlet-driven electroweak phase transition. JHEP **08**, 096 (2017). https://doi.org/10.1007/JHEP08(2017)096. arXiv:1704.05844
18. P. Hernandez, N. Rius, Neutral heavy leptons and electroweak baryogenesis. Nucl. Phys. B **495**, 57–80 (1997). https://doi.org/10.1016/S0550-3213(97)00193-4. arXiv:hep-ph/9611227
19. E. Fernández-Martínez, J. López-Pavón, T. Ota, S. Rosauro-Alcaraz, ν electroweak baryogenesis. JHEP **10**, 063 (2020). https://doi.org/10.1007/JHEP10(2020)063. arXiv:2007.11008
20. M. Carena, Z. Liu, Y. Wang, Electroweak phase transition with spontaneous Z_2-breaking. JHEP **08**, 107 (2020). https://doi.org/10.1007/JHEP08(2020)107. arXiv:1911.10206
21. J.M. Cline, G. Laporte, H. Yamashita, S. Kraml, Electroweak phase transition and LHC signatures in the singlet Majoron model. JHEP **07**, 040 (2009). https://doi.org/10.1088/1126-6708/2009/07/040. arXiv:0905.2559
22. P. Hernández, M. Kekic, J. López-Pavón, J. Racker, J. Salvado, Testable baryogenesis in seesaw models. JHEP **08**, 157 (2016). https://doi.org/10.1007/JHEP08(2016)157. arXiv:1606.06719
23. G. Arcadi, A. Djouadi, M. Raidal, Dark matter through the Higgs portal. Phys. Rep. **842**, 1–180 (2020). https://doi.org/10.1016/j.physrep.2019.11.003. arXiv:1903.03616
24. A. Falkowski, J. Juknevich, J. Shelton, Dark matter through the neutrino portal. arXiv:0908.1790
25. M. Lindner, A. Merle, V. Niro, Enhancing dark matter annihilation into neutrinos. Phys. Rev. D **82**, 123529 (2010). https://doi.org/10.1103/PhysRevD.82.123529. arXiv:1005.3116
26. B. Bertoni, S. Ipek, D. McKeen, A.E. Nelson, Constraints and consequences of reducing small scale structure via large dark matter-neutrino interactions. JHEP **04**, 170 (2015). https://doi.org/10.1007/JHEP04(2015)170. arXiv:1412.3113
27. V. Gonzalez Macias, J. Wudka, Effective theories for Dark Matter interactions and the neutrino portal paradigm. JHEP **07**, 161 (2015). https://doi.org/10.1007/JHEP07(2015)161. arXiv:1506.03825
28. B. Batell, T. Han, D. McKeen, B. Shams Es Haghi, Thermal dark matter through the Dirac neutrino portal. Phys. Rev. D **97**, 075016 (2018). https://doi.org/10.1103/PhysRevD.97.075016. arXiv:1709.07001
29. M. Blennow, E. Fernandez-Martinez, A. Olivares-Del Campo, S. Pascoli, S. Rosauro-Alcaraz, A.V. Titov, Neutrino portals to dark matter. Eur. Phys. J. C **79**, 555 (2019). https://doi.org/10.1140/epjc/s10052-019-7060-5. arXiv:1903.00006
30. M.J. Baker, J. Kopp, A.J. Long, Filtered dark matter at a first order phase transition. Phys. Rev. Lett. **125**, 151102 (2020). https://doi.org/10.1103/PhysRevLett.125.151102. arXiv:1912.02830
31. M.J. Baker, M. Breitbach, J. Kopp, L. Mittnacht, Y. Soreq, Filtered baryogenesis. arXiv:2112.08987
32. P. Minkowski, $\mu \to e\gamma$ at a rate of one out of 10^9 muon decays? Phys. Lett. B **67**, 421–428 (1977). https://doi.org/10.1016/0370-2693(77)90435-X
33. R.N. Mohapatra, G. Senjanovic, Neutrino mass and spontaneous parity nonconservation. Phys. Rev. Lett. **44**, 912 (1980). https://doi.org/10.1103/PhysRevLett.44.912
34. T. Yanagida, Horizontal gauge symmetry and masses of neutrinos. Conf. Proc. C **7902131**, 95–99 (1979)
35. M. Gell-Mann, P. Ramond, R. Slansky, Complex spinors and unified theories. Conf. Proc. C **790927**, 315–321 (1979). arXiv:1306.4669
36. G.C. Branco, W. Grimus, L. Lavoura, The seesaw mechanism in the presence of a conserved lepton number. Nucl. Phys. B **312**, 492 (1989). https://doi.org/10.1016/0550-3213(89)90304-0

37. J. Kersten, AYu. Smirnov, Right-handed neutrinos at CERN LHC and the mechanism of neutrino mass generation. Phys. Rev. D **76**, 073005 (2007). https://doi.org/10.1103/PhysRevD.76.073005. arXiv:0705.3221
38. A. Abada, C. Biggio, F. Bonnet, M.B. Gavela, T. Hambye, Low energy effects of neutrino masses. JHEP **12**, 061 (2007). https://doi.org/10.1088/1126-6708/2007/12/061. arXiv:0707.4058
39. R.N. Mohapatra, Mechanism for understanding small neutrino mass in superstring theories. Phys. Rev. Lett. **56**, 561–563 (1986). https://doi.org/10.1103/PhysRevLett.56.561
40. R.N. Mohapatra, J.W.F. Valle, Neutrino mass and baryon number nonconservation in superstring models. Phys. Rev. D **34**, 1642 (1986). https://doi.org/10.1103/PhysRevD.34.1642
41. E.K. Akhmedov, M. Lindner, E. Schnapka, J.W.F. Valle, Left-right symmetry breaking in NJL approach. Phys. Lett. B **368**, 270–280 (1996). https://doi.org/10.1016/0370-2693(95)01504-3. arXiv:hep-ph/9507275
42. M. Malinsky, J.C. Romao, J.W.F. Valle, Novel supersymmetric SO(10) seesaw mechanism. Phys. Rev. Lett. **95**, 161801 (2005). https://doi.org/10.1103/PhysRevLett.95.161801. arXiv:hep-ph/0506296
43. E. Fernández-Martínez, X. Marcano, D. Naredo-Tuero, HNL mass degeneracy: implications for low-scale seesaws, LNV at colliders and leptogenesis. arXiv:2209.04461
44. S.R. Coleman, E.J. Weinberg, Radiative corrections as the origin of spontaneous symmetry breaking. Phys. Rev. D **7**, 1888–1910 (1973). https://doi.org/10.1103/PhysRevD.7.1888
45. L. Dolan, R. Jackiw, Symmetry behavior at finite temperature. Phys. Rev. D **9**, 3320–3341 (1974). https://doi.org/10.1103/PhysRevD.9.3320
46. S. Weinberg, Gauge and global symmetries at high temperature. Phys. Rev. D **9**, 3357–3378 (1974). https://doi.org/10.1103/PhysRevD.9.3357
47. H.H. Patel, M.J. Ramsey-Musolf, Baryon washout, electroweak phase transition, and perturbation theory. JHEP **07**, 029 (2011). https://doi.org/10.1007/JHEP07(2011)029. arXiv:1101.4665
48. D. Croon, O. Gould, P. Schicho, T.V.I. Tenkanen, G. White, Theoretical uncertainties for cosmological first-order phase transitions. JHEP **04**, 055 (2021). https://doi.org/10.1007/JHEP04(2021)055. arXiv:2009.10080
49. A. Papaefstathiou, G. White, The electro-weak phase transition at colliders: confronting theoretical uncertainties and complementary channels. JHEP **05**, 099 (2021). https://doi.org/10.1007/JHEP05(2021)099. arXiv:2010.00597
50. K. Kajantie, M. Laine, K. Rummukainen, M.E. Shaposhnikov, Generic rules for high temperature dimensional reduction and their application to the standard model. Nucl. Phys. B **458**, 90–136 (1996). https://doi.org/10.1016/0550-3213(95)00549-8. arXiv:hep-ph/9508379
51. T. Brauner, T.V.I. Tenkanen, A. Tranberg, A. Vuorinen, D.J. Weir, Dimensional reduction of the Standard Model coupled to a new singlet scalar field. JHEP **03**, 007 (2017). https://doi.org/10.1007/JHEP03(2017)007. arXiv:1609.06230
52. P.M. Schicho, T.V.I. Tenkanen, J. Österman, Robust approach to thermal resummation: Standard Model meets a singlet. JHEP **06**, 130 (2021). https://doi.org/10.1007/JHEP06(2021)130. arXiv:2102.11145
53. L. Niemi, P. Schicho, T.V.I. Tenkanen, Singlet-assisted electroweak phase transition at two loops. Phys. Rev. D **103**, 115035 (2021). https://doi.org/10.1103/PhysRevD.103.115035. arXiv:2103.07467
54. P. Schicho, T.V.I. Tenkanen, G. White, Combining thermal resummation and gauge invariance for electroweak phase transition. arXiv:2203.04284
55. K. Fuyuto, E. Senaha, Improved sphaleron decoupling condition and the Higgs coupling constants in the real singlet-extended standard model. Phys. Rev. D **90**, 015015 (2014). https://doi.org/10.1103/PhysRevD.90.015015. arXiv:1406.0433
56. A.V. Kotwal, M.J. Ramsey-Musolf, J.M. No, P. Winslow, Singlet-catalyzed electroweak phase transitions in the 100 TeV frontier. Phys. Rev. D **94**, 035022 (2016). https://doi.org/10.1103/PhysRevD.94.035022. arXiv:1605.06123
57. K. Hashino, M. Kakizaki, S. Kanemura, P. Ko, T. Matsui, Gravitational waves and Higgs boson couplings for exploring first order phase transition in the model with a singlet scalar field. Phys. Lett. B **766**, 49–54 (2017). https://doi.org/10.1016/j.physletb.2016.12.052. arXiv:1609.00297
58. G. Kurup, M. Perelstein, Dynamics of electroweak phase transition in singlet-scalar extension of the standard model. Phys. Rev. D **96**, 015036 (2017). https://doi.org/10.1103/PhysRevD.96.015036. arXiv:1704.03381
59. C.-W. Chiang, Y.-T. Li, E. Senaha, Revisiting electroweak phase transition in the standard model with a real singlet scalar. Phys. Lett. B **789**, 154–159 (2019). https://doi.org/10.1016/j.physletb.2018.12.017. arXiv:1808.01098
60. J. Kozaczuk, M.J. Ramsey-Musolf, J. Shelton, Exotic Higgs boson decays and the electroweak phase transition. Phys. Rev. D **101**, 115035 (2020). https://doi.org/10.1103/PhysRevD.101.115035. arXiv:1911.10210
61. W. Liu, K.-P. Xie, Probing electroweak phase transition with multi-TeV muon colliders and gravitational waves. JHEP **04**, 015 (2021). https://doi.org/10.1007/JHEP04(2021)015. arXiv:2101.10469
62. M. Carena, J. Kozaczuk, Z. Liu, T. Ou, M.J. Ramsey-Musolf, J. Shelton et al., Probing the electroweak phase transition with exotic Higgs decays. In *2022 Snowmass Summer Study*, 3 (2022). arXiv:2203.08206
63. A. Azatov, G. Barni, S. Chakraborty, M. Vanvlasselaer, W. Yin, Ultra-relativistic bubbles from the simplest Higgs portal and their cosmological consequences. JHEP **10**, 017 (2022). https://doi.org/10.1007/JHEP10(2022)017. arXiv:2207.02230
64. Particle Data Group Collaboration, R.L. Workman, Review of Particle Physics. PTEP **2022**, 083C01 (2022)
65. CDF Collaboration, T. Aaltonen et al., High-precision measurement of the W boson mass with the CDF II detector. Science **376**, 170–176 (2022). https://doi.org/10.1126/science.abk1781
66. M. Blennow, P. Coloma, E. Fernández-Martínez, M. González-López, Right-handed neutrinos and the CDF II anomaly. arXiv:2204.04559
67. E. Fernandez-Martinez, J. Hernandez-Garcia, J. Lopez-Pavon, Global constraints on heavy neutrino mixing. JHEP **08**, 033 (2016). https://doi.org/10.1007/JHEP08(2016)033. arXiv:1605.08774
68. D. Naredo-Tuero, Private communication for updated results. Work in progress
69. P.D. Bolton, F.F. Deppisch, P.S. Bhupal Dev, Neutrinoless double beta decay versus other probes of heavy sterile neutrinos. JHEP **03**, 170 (2020). https://doi.org/10.1007/JHEP03(2020)170. arXiv:1912.03058
70. M. Hostert, Heavy Neutrino Limits GitHub repository. https://github.com/mhostert/Heavy-Neutrino-Limits
71. ATLAS Collaboration, G. Aad et al., Combined measurements of Higgs boson production and decay using up to 80 fb^{-1} of proton–proton collision data at $\sqrt{s} = 13$ TeV collected with the ATLAS experiment. Phys. Rev. D **101**, 012002 (2020). https://doi.org/10.1103/PhysRevD.101.012002. arXiv:1909.02845
72. CMS Collaboration, Combined Higgs boson production and decay measurements with up to 137 fb^{-1} of proton–proton collision data at $\sqrt{s} = 13$ TeV
73. T. Robens, T. Stefaniak, Status of the Higgs singlet extension of the standard model after LHC Run 1. Eur. Phys. J. C **75**,

104 (2015). https://doi.org/10.1140/epjc/s10052-015-3323-y. arXiv:1501.02234
74. D. Buttazzo, F. Sala, A. Tesi, Singlet-like Higgs bosons at present and future colliders. JHEP **11**, 158 (2015). https://doi.org/10.1007/JHEP11(2015)158. arXiv:1505.05488
75. E. Fuchs, O. Matsedonskyi, I. Savoray, M. Schlaffer, Collider searches for scalar singlets across lifetimes. JHEP **04**, 019 (2021). https://doi.org/10.1007/JHEP04(2021)019. arXiv:2008.12773
76. S. Dawson, P.P. Giardino, S. Homiller, Uncovering the High Scale Higgs Singlet Model. Phys. Rev. D **103**, 075016 (2021). https://doi.org/10.1103/PhysRevD.103.075016. arXiv:2102.02823
77. ATLAS Collaboration, A detailed map of Higgs boson interactions by the ATLAS experiment ten years after the discovery. Nature **607**, 52–59 (2022). https://doi.org/10.1038/s41586-022-04893-w. arXiv:2207.00092
78. CMS Collaboration, A portrait of the Higgs boson by the CMS experiment ten years after the discovery. Nature **607**, 60–68 (2022). https://doi.org/10.1038/s41586-022-04892-x. arXiv:2207.00043
79. G.J. Feldman, R.D. Cousins, A unified approach to the classical statistical analysis of small signals. Phys. Rev. D **57**, 3873–3889 (1998). https://doi.org/10.1103/PhysRevD.57.3873. arXiv:physics/9711021
80. A. Das, Y. Gao, T. Kamon, Heavy neutrino search via semileptonic Higgs decay at the LHC. Eur. Phys. J. C **79**, 424 (2019). https://doi.org/10.1140/epjc/s10052-019-6937-7. arXiv:1704.00881
81. A. Das, P.S.B. Dev, C.S. Kim, Constraining sterile neutrinos from precision Higgs data. Phys. Rev. D **95**, 115013 (2017). https://doi.org/10.1103/PhysRevD.95.115013. arXiv:1704.00880
82. LHC Higgs Working Group, https://twiki.cern.ch/twiki/bin/view/LHCPhysics/LHCHWG
83. ATLAS Collaboration, G. Aad et al., Search for heavy resonances decaying into a pair of Z bosons in the $\ell^+\ell^-\ell'^+\ell'^-$ and $\ell^+\ell^-\nu\bar{\nu}$ final states using 139 fb^{-1} of proton–proton collisions at $\sqrt{s} = 13$ TeV with the ATLAS detector. Eur. Phys. J. C **81**, 332 (2021). https://doi.org/10.1140/epjc/s10052-021-09013-y. arXiv:2009.14791
84. M.L. Graesser, Experimental constraints on Higgs boson decays to TeV-scale right-handed neutrinos. arXiv:0705.2190
85. A. Caputo, P. Hernandez, J. Lopez-Pavon, J. Salvado, The seesaw portal in testable models of neutrino masses. JHEP **06**, 112 (2017). https://doi.org/10.1007/JHEP06(2017)112. arXiv:1704.08721
86. M. Gorbahn, J.M. No, V. Sanz, Benchmarks for Higgs effective theory: extended Higgs sectors. JHEP **10**, 036 (2015). https://doi.org/10.1007/JHEP10(2015)036. arXiv:1502.07352
87. A. Beniwal, M. Lewicki, M. White, A.G. Williams, Gravitational waves and electroweak baryogenesis in a global study of the extended scalar singlet model. JHEP **02**, 183 (2019). https://doi.org/10.1007/JHEP02(2019)183. arXiv:1810.02380
88. M.E. Peskin, T. Takeuchi, Estimation of oblique electroweak corrections. Phys. Rev. D **46**, 381–409 (1992). https://doi.org/10.1103/PhysRevD.46.381
89. J. Haller, A. Hoecker, R. Kogler, K. Mönig, T. Peiffer, J. Stelzer, Update of the global electroweak fit and constraints on two-Higgs-doublet models. Eur. Phys. J. C **78**, 675 (2018). https://doi.org/10.1140/epjc/s10052-018-6131-3. arXiv:1803.01853
90. W. Loinaz, N. Okamura, T. Takeuchi, L.C.R. Wijewardhana, The NuTeV anomaly, neutrino mixing, and a heavy Higgs boson. Phys. Rev. D **67**, 073012 (2003). https://doi.org/10.1103/PhysRevD.67.073012. arXiv:hep-ph/0210193
91. W. Loinaz, N. Okamura, S. Rayyan, T. Takeuchi, L.C.R. Wijewardhana, The NuTeV anomaly, lepton universality, and nonuniversal neutrino gauge couplings. Phys. Rev. D **70**, 113004 (2004). https://doi.org/10.1103/PhysRevD.70.113004. arXiv:hep-ph/0403306
92. E. Akhmedov, A. Kartavtsev, M. Lindner, L. Michaels, J. Smirnov, Improving electro-weak fits with TeV-scale sterile neutrinos. JHEP **05**, 081 (2013). https://doi.org/10.1007/JHEP05(2013)081. arXiv:1302.1872
93. E. Fernandez-Martinez, J. Hernandez-Garcia, J. Lopez-Pavon, M. Lucente, Loop level constraints on Seesaw neutrino mixing. JHEP **10**, 130 (2015). https://doi.org/10.1007/JHEP10(2015)130. arXiv:1508.03051
94. CMS Collaboration, S. Chatrchyan et al., Measurement of Higgs boson production and properties in the WW decay channel with leptonic final states. JHEP **01**, 096 (2014). https://doi.org/10.1007/JHEP01(2014)096. arXiv:1312.1129
95. ATLAS Collaboration, G. Aad et al., Search for an additional, heavy Higgs boson in the $H \to ZZ$ decay channel at $\sqrt{s} = 8$ TeV in pp collision data with the ATLAS detector. Eur. Phys. J. C **76**, 45 (2016). https://doi.org/10.1140/epjc/s10052-015-3820-z. arXiv:1507.05930
96. ALEPH Collaboration, A. Heister et al., Final results of the searches for neutral Higgs bosons in e+ e- collisions at s**(1/2) up to 209-GeV. Phys. Lett. B **526**, 191–205 (2002). https://doi.org/10.1016/S0370-2693(01)01487-3. arXiv:hep-ex/0201014
97. DELPHI Collaboration, J. Abdallah et al., Searches for invisibly decaying Higgs bosons with the DELPHI detector at LEP. Eur. Phys. J. C **32**, 475–492 (2004). https://doi.org/10.1140/epjc/s2003-01469-8. arXiv:hep-ex/0401022
98. L3 Collaboration, P. Achard et al., Search for an invisibly-decaying Higgs boson at LEP. Phys. Lett. B **609**, 35–48 (2005). https://doi.org/10.1016/j.physletb.2005.01.030. arXiv:hep-ex/0501033
99. OPAL Collaboration, G. Abbiendi et al., Search for invisibly decaying Higgs bosons in e+ e− —> Z0 h0 production at s**(1/2) = 183-GeV–209-GeV. Phys. Lett. B **682**, 381–390 (2010). https://doi.org/10.1016/j.physletb.2009.09.010. arXiv:0707.0373
100. ATLAS Collaboration, G. Aad et al., Search for Higgs boson pair production in the two bottom quarks plus two photons final state in pp collisions at $\sqrt{s} = 13$ TeV with the ATLAS detector. Phys. Rev. D **106**, 052001 (2022). https://doi.org/10.1103/PhysRevD.106.052001. arXiv:2112.11876
101. ATLAS Collaboration, Search for resonant and non-resonant Higgs boson pair production in the $b\bar{b}\tau^+\tau^-$ decay channel using 13 TeV pp collision data from the ATLAS detector. arXiv:2209.10910
102. B.W. Lee, C. Quigg, H.B. Thacker, Weak interactions at very high-energies: the role of the Higgs boson mass. Phys. Rev. D **16**, 1519 (1977). https://doi.org/10.1103/PhysRevD.16.1519
103. M. Mitra, R. Ruiz, D.J. Scott, M. Spannowsky, Neutrino jets from high-mass W_R gauge bosons in TeV-scale left-right symmetric models. Phys. Rev. D **94**, 095016 (2016). https://doi.org/10.1103/PhysRevD.94.095016. arXiv:1607.03504
104. O. Mattelaer, M. Mitra, R. Ruiz, Automated neutrino jet and top jet predictions at next-to-leading-order with parton shower matching in effective left-right symmetric models. arXiv:1610.08985
105. C. Degrande, O. Mattelaer, R. Ruiz, J. Turner, Fully-automated precision predictions for heavy neutrino production mechanisms at hadron colliders. Phys. Rev. D **94**, 053002 (2016). https://doi.org/10.1103/PhysRevD.94.053002. [arXiv:1602.06957]
106. CMS Collaboration, Search for Z′ bosons decaying to pairs of heavy Majorana neutrinos in proton-proton collisions at $\sqrt{s} =$ 13 TeV
107. Y. Cai, T. Han, T. Li, R. Ruiz, Lepton number violation: seesaw models and their collider tests. Front. Phys. **6**, 40 (2018). https://doi.org/10.3389/fphy.2018.00040. arXiv:1711.02180
108. T. Han, J. Liao, H. Liu, D. Marfatia, R. Ruiz, BSM ν physics: complementarity across energies—a white paper for Snowmass 2021. In *2022 Snowmass Summer Study*, 3 (2022). arXiv:2203.06131

109. CMS Collaboration, A.M. Sirunyan et al., Combination of searches for Higgs boson pair production in proton–proton collisions at $\sqrt{s} = 13$ TeV. Phys. Rev. Lett. **122**, 121803 (2019). https://doi.org/10.1103/PhysRevLett.122.121803. arXiv:1811.09689
110. ATLAS Collaboration, G. Aad et al., Combination of searches for Higgs boson pairs in pp collisions at $\sqrt{s}$ =13 TeV with the ATLAS detector. Phys. Lett. B **800**, 135103 (2020). https://doi.org/10.1016/j.physletb.2019.135103. arXiv:1906.02025
111. ATLAS Collaboration Collaboration, Combination of searches for non-resonant and resonant Higgs boson pair production in the $b\bar{b}\gamma\gamma$, $b\bar{b}\tau^+\tau^-$ and $b\bar{b}b\bar{b}$ decay channels using pp collisions at $\sqrt{s}$ = 13 TeV with the ATLAS detector, Tech. rep. (CERN, Geneva, 2021)
112. G.C. Dorsch, S.J. Huber, K. Mimasu, J.M. No, The Higgs vacuum uplifted: revisiting the electroweak phase transition with a second Higgs doublet. JHEP **12**, 086 (2017). https://doi.org/10.1007/JHEP12(2017)086. arXiv:1705.09186
113. M. Carena, Z. Liu, M. Riembau, Probing the electroweak phase transition via enhanced di-Higgs boson production. Phys. Rev. D **97**, 095032 (2018). https://doi.org/10.1103/PhysRevD.97.095032. arXiv:1801.00794
114. F. Arco, S. Heinemeyer, M. Mühlleitner, K. Radchenko, Sensitivity to triple Higgs couplings via di-Higgs production in the 2HDM at the (HL-)LHC. arXiv:2212.11242
115. M. Blennow, E. Fernandez-Martinez, Neutrino oscillation parameter sampling with MonteCUBES. Comput. Phys. Commun. **181**, 227–231 (2010). https://doi.org/10.1016/j.cpc.2009.09.014. arXiv:0903.3985
116. M. Quiros, Finite temperature field theory and phase transitions. In *ICTP Summer School in High-Energy Physics and Cosmology*, pp. 187–259 (1999). arXiv:hep-ph/9901312
117. T. Biekötter, S. Heinemeyer, J.M. No, M.O. Olea, G. Weiglein, Fate of electroweak symmetry in the early Universe: non-restoration and trapped vacua in the N2HDM. JCAP **06**, 018 (2021). https://doi.org/10.1088/1475-7516/2021/06/018. arXiv:2103.12707
118. S. Baum, M. Carena, N.R. Shah, C.E.M. Wagner, Y. Wang, Nucleation is more than critical: a case study of the electroweak phase transition in the NMSSM. JHEP **03**, 055 (2021). https://doi.org/10.1007/JHEP03(2021)055. arXiv:2009.10743
119. S.R. Coleman, F. De Luccia, Gravitational effects on and of vacuum decay. Phys. Rev. D **21**, 3305 (1980). https://doi.org/10.1103/PhysRevD.21.3305
120. A. Ivanov, A. Ivanov, M. Matteini, M. Matteini, M. Nemevšek, M. Nemevšek et al., Analytic thin wall false vacuum decay rate. JHEP **03**, 209 (2022). https://doi.org/10.1007/JHEP03(2022)209. arXiv:2202.04498
121. C.L. Wainwright, CosmoTransitions: computing cosmological phase transition temperatures and bubble profiles with multiple fields. Comput. Phys. Commun. **183**, 2006–2013 (2012). https://doi.org/10.1016/j.cpc.2012.04.004. arXiv:1109.4189
122. P. Athron, C. Balázs, M. Bardsley, A. Fowlie, D. Harries, G. White, BubbleProfiler: finding the field profile and action for cosmological phase transitions. Comput. Phys. Commun. **244**, 448–468 (2019). https://doi.org/10.1016/j.cpc.2019.05.017. arXiv:1901.03714
123. V. Guada, M. Nemevšek, M. Pintar, FindBounce: package for multi-field bounce actions. Comput. Phys. Commun. **256**, 107480 (2020). https://doi.org/10.1016/j.cpc.2020.107480. arXiv:2002.00881
124. A.D. Linde, Fate of the false vacuum at finite temperature: theory and applications. Phys. Lett. B **100**, 37–40 (1981). https://doi.org/10.1016/0370-2693(81)90281-1
125. G.W. Anderson, L.J. Hall, The electroweak phase transition and baryogenesis. Phys. Rev. D **45**, 2685–2698 (1992). https://doi.org/10.1103/PhysRevD.45.2685
126. L.D. McLerran, M.E. Shaposhnikov, N. Turok, M.B. Voloshin, Why the baryon asymmetry of the universe is approximately 10**-10. Phys. Lett. B **256**, 451–456 (1991). https://doi.org/10.1016/0370-2693(91)91794-V
127. M. Dine, P. Huet, R.L. Singleton Jr., Baryogenesis at the electroweak scale. Nucl. Phys. B **375**, 625–648 (1992). https://doi.org/10.1016/0550-3213(92)90113-P
128. S.R. Coleman, Quantum tunneling and negative eigenvalues. Nucl. Phys. B **298**, 178–186 (1988). https://doi.org/10.1016/0550-3213(88)90308-2
129. J.M. Cline, G.D. Moore, G. Servant, Was the electroweak phase transition preceded by a color broken phase? Phys. Rev. D **60**, 105035 (1999). https://doi.org/10.1103/PhysRevD.60.105035. arXiv:hep-ph/9902220
130. J.R. Espinosa, T. Konstandin, A fresh look at the calculation of tunneling actions in multi-field potentials. JCAP **01**, 051 (2019). https://doi.org/10.1088/1475-7516/2019/01/051. arXiv:1811.09185
131. S. Akula, C. Balázs, G.A. White, Semi-analytic techniques for calculating bubble wall profiles. Eur. Phys. J. C **76**, 681 (2016). https://doi.org/10.1140/epjc/s10052-016-4519-5. arXiv:1608.00008
132. M. Cepeda et al., Report from Working Group 2: Higgs Physics at the HL-LHC and HE-LHC. CERN Yellow Rep. Monogr. **7**, 221–584 (2019). https://doi.org/10.23731/CYRM-2019-007.221. arXiv:1902.00134